AD

Research and Development Technical Report

ECOM-0082-F

STUDIES OF BOUNDARY-LAYER PARAMETERS

By

H. H. Lettau, Principal Investigator;
Charles R. Stearns, Co-Investigator;

and

Kenneth MacKay

July 1970

ECOM

UNITED STATES ARMY ELECTRONICS COMMAND
ATMOSPHERIC SCIENCES LABORATORY
FORT HUACHUCA, ARIZONA

Contract DAEA-18-60-C-0082
The University of Wisconsin
Madison, Wisconsin

NOTICES

Citation of trade names and names of manufacturers in this report is not to be construed as official government indorsement or approval of commercial products or services references.

The findings in this report are not to be construed as an official Department of Army position unless so designated by other authorized documents.

Destroy this report when it is no longer needed.

TR ECOM-0082-F
July 1970

Reports Control Symbol
OSD-1366

STUDIES OF BOUNDARY-LAYER PARAMETERS

Final Report

Contract DAEA-18-69-0082
DA Task 1T061102-B53A-17

Prepared by

H. H. Lettau, Principal Investigator;
Charles R. Stearns, Co-Investigator;
and
Kenneth MacKay

Department of Meteorology
The University of Wisconsin
Madison, Wisconsin

for

U. S. Army Electronics Command
Atmospheric Sciences Laboratory
Fort Huachuca, Arizona

Scanner's note:

This page is blank.

GENERAL INTRODUCTION

The technical requirements for contract No. DAEA 18-69-C-0082 request a study of certain boundary-layer parameters utilizing the Davis data. Specifically, the technical requirements request the value of $N_Q = K_h K_m^{-1}$, $N_E = K_w K_m^{-1}$, an expression for the wind profile and possible confirmation of anomalies in the "Davis Data."

Section 1 entitled "Note on Eddy Diffusivities" by H. H. Lettau uses theoretical developments to show that N_Q may be equal to one only near adiabatic conditions. The same may be true for N_E. Section 3 entitled "The Effect of Time-Variable Fluxes on Mean Wind and Temperature Structure" by C. R. Stearns shows the effect on mean profile structure and on N_Q of averaging periods with high or low stress and/or high or low heat flux density. Sections 1 and 3 give reasons for difficulty in determining consistent values of N_Q and N_E.

Section 4 entitled "Intercomparison of Flux Densities of Heat, Moisture and Momentum at Davis, California, 1970" by C. R. Stearns shows that the results obtained by assuming $N_Q = N_E = \phi^{-1/2}$ are reasonable when compared to the shear-stress and weighing lysimeters. The scatter of the data points awaits explanation.

The problem of profile structure is part of Sections 3 and 4. In analyzing the data for Section 4, a measure of the fit to profiles of wind temperature and moisture was obtained but not presented. This information will be published in the future.

The anomalies in wind direction at various levels have not been resolved and appear to be impossible because the wind vanes operated poorly at low wind speeds when the greatest vertical difference would occur. The horizontal stress, heat flux and moisture flux differences between masts appear to be real and will also be the subject of future publication.

Charles R. Stearns
Madison, Wisconsin

Scanner's note:

This page is blank.

CONTENTS

Scanner's note:

This page is blank.

NOTE ON EDDY DIFFUSIVITIES

H. Lettau
University of Wisconsin at Madison

1. Defining Relations

Consider fully developed turbulence in flow where the lower fluid boundary coincides with the horizontal x, y-plane at $z = 0$. Of interest are the eddy fluxes in the direction normal to the boundary, which is also taken to be the direction perpendicular to the mean stream lines. Of primary importance is the eddy flux of momentum per unit mass. Next important are the simultaneous fluxes of various scalar properties, or specific admixtures per unit mass. All these fluxes are physically related to boundary transfer of momentum (that is, the surface stress) and simultaneous area sources (or sinks) of admixtures, like surface release of heat, or moisture, etc. Let the overbar indicate a suitably defined average of fluid variables at a point. In most practical applications we use a time-mean of either x-momentum or y-momentum per unit mass (that is, of horizontal flow components u or v), and likewise of fluid admixture, s. The Reynolds tensor yields the defining equations of the eddy fluxes. Specifically, when w' denotes the fluctuating component of fluid motion normal to the boundary (with $\overline{w'} = 0$, but $\overline{w'w'}$ significantly positive) the eddy fluxes of interest are given by the covariances (mixed products) $\overline{w'u}$, $\overline{w'v}$, $\overline{w's}$. Note that under the assumptions of ordinary turbulence statistics, $\overline{w'u} = \overline{w'u'}$ and $\overline{w's} = \overline{w's'}$, etc. In the following, we shall use the simpler writing $\overline{w'u}$ or $\overline{w's}$, instead of $\overline{w'u'}$ and $\overline{w's'}$, and corresponding simplifications in other eddy covariances.

Let the subscripts x, y, z denote partial differentiation of a dependent variable with respect to the cartesian coordinates (which are the only independent variables of steady mean states). We consider turbulent flow in which eddy fluxes occur only in the direction (z) perpendicular to the lower boundary. Then the eddy diffusivities for any specified fluid property are formally defined as follows:

$$(1.1) \qquad K(u) = -\overline{w'u}/\overline{u}_z \; ; \quad K(v) = -\overline{w'v}/\overline{v}_z \; ; \quad K(s) = -\overline{w's}/\overline{s}_z \; .$$

Beginning with pioneer work by Reynolds and Boussinesq, around the turn of the century, many investigators have attempted to explain the physical nature of the coefficients in (1.1). However, it is generally conceded that

there are still unsolved problems, if we want to know more than the trivial fact that for existing eddy fluxes these K's will have nonzero values and physical dimensions of "length" times "velocity" or, specifically, cm^2/sec. Of fundamental importance is the question whether or not (1.1) yields always positive coefficient values, and for what reason we should exclude $\pm$ infinity and or permit negative values; reference is made to Starr (1968). Furthermore, if the K's should always be positive, another question is whether or not they agree with each other when eddy fluxes of different fluid properties coexist at the same point of the turbulent flow. Specifically, it is most important to know whether or not the eddy diffusivity for momentum K(M)--which may be represented either by K(u) or K(v) in (1.1)—equals the eddy diffusivity K(s), for which a specific case is the eddy diffusivity for heat, K(H).

A brief and rather formal discussion of structure of eddy fluxes and eddy diffusivities follows, based on the universal hypothesis for the relationships between mean and eddy states introduced by Lettau (1967). The three-dimensional form of this relationship is given by:

$$(1.2)\qquad \underset{\rightarrow}{V}' = \underset{\rightarrow}{r}' \times [\nabla \times \bar{\underset{\rightarrow}{V}}] - \overline{\underset{\rightarrow}{V} - \underset{\rightarrow}{V}_{ref}} \times [\nabla \times \underset{\rightarrow}{r}'] - \overline{\underset{\rightarrow}{V} - \underset{\rightarrow}{V}_{ref}}(\nabla \cdot \underset{\rightarrow}{r}'),$$

$$(1.3)\qquad s' = -\underset{\rightarrow}{r}' \cdot \nabla \bar{s} - \overline{s - s_{ref}}(\nabla \cdot \underset{\rightarrow}{r}'),$$

where $\underset{\rightarrow}{V}' = \underset{\rightarrow}{i}u' + \underset{\rightarrow}{j}v' + \underset{\rightarrow}{k}w'$, and $\underset{\rightarrow}{r}' = \underset{\rightarrow}{i}x' + \underset{\rightarrow}{j}y' + \underset{\rightarrow}{k}z'$ are the three-dimensional vectors of eddy velocity and eddy displacement, respectively, with $\bar{\underset{\rightarrow}{V}}' = \bar{\underset{\rightarrow}{r}}' = 0$; the subscript "ref" denotes reference values which are constant parameters for a given case of turbulent flow. In comparison with the version given in Lettau (1967), the only difference is the consideration of $\bar{\underset{\rightarrow}{V}}_{ref}$ in (1.2).

For the sake of clarifying the principles, the following discussion will be restricted to steady, homogeneous (in x and y), and unidirectional mean flow with strictly one-dimensional mean shear (in z only). This implies that among the various averaged fluid variables, only $\bar{u}$, $\bar{u}_z$, $\bar{u}_{zz}$, etc., also $\bar{s}$, $\bar{s}_z$, $\bar{s}_{zz}$, etc., are nonzero, while $\bar{u}_x = \bar{u}_y = \bar{s}_x = \bar{s}_y = \bar{v} = 0$. Because only the eddy velocities in the x and z directions will be considered, we omit also for brevity any consideration of eddy velocity in the horizontal cross-stream direction, although v' exists and the significantly positive $\overline{v'v'}$ can be calculated with the aid of (1.2) even for $\bar{\underset{\rightarrow}{V}} = \underset{\rightarrow}{i}\bar{u}$, and $\bar{\underset{\rightarrow}{V}}_{ref} = \underset{\rightarrow}{i}\bar{u}_{ref}$. Correspondingly, we omit consideration of the component y' of eddy displacements, and any covariances involving y' or its derivatives. In summary, the relevant components u', w', and s', are expressed as the following special versions of (1.2) and (1.3):

$$(1.4) \qquad u' = -\bar{u}_z z' - \overline{u-u}_{ref}(x'_x + z'_z),$$

$$(1.5) \qquad w' = \bar{u}_z x' - \overline{u-u}_{ref}(x'_z - z'_x),$$

$$(1.6) \qquad s' = -\bar{s}_z z' - \overline{s-s}_{ref}(x'_x + z'_z).$$

In (1.4) and (1.6), the first members are the "gradient terms," the second members the "divergence terms." In (1.5), both members are vorticity terms, depending on the curl of mean velocity, and the curl of the eddy displacement vector. Hence, the system (1.4) to (1.6) expresses the vortex-nature of flux producing eddies in turbulent flow; see Lettau (1964, 1967).

By definition of the Reynolds averages it follows that $\overline{w'u'} = \overline{w'u}$, and $\overline{w's'} = \overline{w's}$. Hence, the eddy fluxes are obtained from (1.4) to (1.6),

$$(1.7) \qquad -\overline{w'u} = \overline{x'z'}\,\bar{u}_z\bar{u}_z + (\overline{x'_x x'} + \overline{z'_x z'} + \overline{z'_z x'} - \overline{x'_z z'})\,\bar{u}_z\,\overline{u-u}_{ref}$$

$$- (\overline{x'_x x'_z} - \overline{z'_x z'_z} + \overline{x'_z z'_z} - \overline{x'_x z'_x})\,(\overline{u-u}_{ref})^2$$

$$(1.8) \qquad -\overline{w's} = \overline{x'z'}\,\bar{u}_z\bar{s}_z + (\overline{z'_z x'} + \overline{x'_x x'})\,\bar{u}_z\,\overline{s-s}_{ref} - (\overline{x'_z z'} - \overline{z'_x z'})\,\bar{s}_z\,\overline{u-u}_{ref}$$

$$- (\overline{x'_x x'_z} - \overline{z'_x z'_z} + \overline{x'_z z'_z} - \overline{x'_x z'_x})\,\overline{u-u}_{ref}\,\overline{s-s}_{ref}.$$

By definition (1.1), the fluxes yield the eddy diffusivities of momentum (u, or x-momentum per unit mass) and scalar admixture (s, per unit mass),

$$(1.9) \qquad K(u) = \overline{x'z'}\,\bar{u}_z + (\overline{x'_x x'} + \overline{z'_x z'} + \overline{z'_z x'} - \overline{x'_z z'})\,\overline{u-u}_{ref}$$

$$- (\overline{x'_x x'_z} - \overline{z'_x z'_z} + \overline{x'_z z'_z} - \overline{x'_x z'_x})\,(\overline{u-u}_{ref})^2/\bar{u}_z,$$

$$(1.10) \quad K(s) = \overline{x'z'}\,\bar{u}_z + (\overline{z'_z x'} + \overline{x'_x x'})\,\bar{u}_z\,\overline{s-s}_{ref}/\bar{s}_z - (\overline{x'_z z'} - \overline{z'_x z'})\,\overline{u-u}_{ref}$$

$$- (\overline{x'_x x'_z} - \overline{z'_x z'_z} + \overline{x'_z z'_z} - \overline{x'_x z'_x})\,\overline{u-u}_{ref}\,\overline{s-s}_{ref}/\bar{s}_z$$

Obviously, only the first members of Eqs. (19) and (1.10) are the same. It appears that either K-value may fall between zero and $\pm$ infinity. This variability is due partly to the "mean-state terms" $\bar{u}_z$, $\bar{s}_z$, $\overline{u-u}_{ref}$, and $\overline{s-s}_{ref}$, and partly due to the eddy structure terms. The latter

contribution is of major importance and shall be investigated in the following. With regard to "mean-state terms" the consequence of the appearance of finite reference values, while $\overline{u-u_{ref}} \neq 0$ and $\overline{s-s_{ref}} \neq 0$, documents that the ideal of strictly "gradient flux" or gradient diffusion must have very definite limitations.

2. Hierarchy of Simplified Eddy Flux Models

2.1 Horizontal Homogeneity of Eddy Structure

A first step towards simplification of the eddy flux model (1.7) and (1.8) is to assume that structure variances and covariances share with mean flow variables the feature of independency on the horizontal coordinates x and y. This implies that

$$(2.1) \qquad \overline{x'x'}_x = \frac{1}{2}(\overline{x'x'})_x = \overline{z'z'}_x = \frac{1}{2}(\overline{z'z'})_x = 0.$$

This produces the following simplification of (1.7) and (1.8),

$$(2.2) \qquad -\overline{w'u} = \overline{x'z'}\,\bar{u}_z\,\bar{u}_z - (\overline{x'z'}_z - \overline{z'x'}_z)\,\bar{u}_z\,\overline{u-u_{ref}}$$
$$- (\overline{x'x'}_{xz} - \overline{z'z'}_{xz} + \overline{x'z'}_{zz} - \overline{x'z'}_{xx})\,\overline{(u-u_{ref})^2},$$

$$(2.3) \qquad -\overline{w's} = \overline{x'z'}\,\bar{u}_z\,\bar{s}_z - (\overline{x'z'}_z\,\bar{s}_z\,\overline{u-u_{ref}} + \overline{z'x'}_z\,\bar{u}_z\,\overline{s-s_{ref}}$$
$$- (\overline{x'x'}_{xz} - \overline{z'z'}_{xz} + \overline{x'z'}_{zz} - \overline{x'z'}_{xx})\,\overline{u-u_{ref}}\;\overline{s-s_{ref}}.$$

The corresponding forms for K(u) and K(s) can readily be derived and need not be written down. Obviously, the simplification (2.1) does neither result in strictly gradient diffusion nor does it produce equality of eddy diffusivities. On the other hand, it may be remarked that the variances $\overline{x'x'}$ and $\overline{z'z'}$ will exist and must be functions of height, that is, $(\overline{x'x'})_z = 2\overline{x'_z x'} \neq 0$, also $(\overline{z'z'})_z = 2\overline{z'_z z'} \neq 0$, in supplement of (2.1). It follows with the aid of (1.4) to (1.6) that these "longitudinal eddy length-scales" express essentially the variances $\overline{w'w'}$, $\overline{u'u'}$, and $\overline{s's'}$. According to Lettau (1968) the longitudinal length-scale controls also the eddy fluxes in free turbulence of inertial jet flows. However, for the problem under discussion, they can be ignored.

2.2 Vertical Coherence (Non-Intermittancy) of Eddy Displacements

It will be assumed that the eddy displacement components x' and z' satisfy the requirement of vertical coherence if

$$\overline{x'_x x'_z} = \overline{z'_x z'_z} = 0. \tag{2.4}$$

The terminology is chosen because it can be shown that (2.4) implies an existing coherence between the simultaneous quasi-harmonic eddy fluctuations of x' and z'. To show this, let A and B denote mean amplitudes, β a characteristic lag constant, and φ' a continuous independent variable related to either time or one of the horizontal coordinates, so that application of the Reynolds average yields $\overline{\sin\varphi'} = \overline{\cos\varphi'} = \overline{\sin\varphi'\cos\varphi'} = 0$, while $\overline{\sin^2\varphi'} = \overline{\cos^2\varphi'} = 1/2$. Let

$$x' = A\sin\varphi; \quad z' = B\sin(\varphi' + \beta), \tag{2.5}$$

so that

$$\overline{x'} = \overline{z'} = 0; \quad \overline{x'x'} = A^2/2; \quad \overline{z'z'} = B^2/2; \quad \overline{x'z'} = \frac{1}{2}AB\cos\beta\,. \tag{2.6}$$

The assumption of homogeneity discussed in Section 2.1 requires that $A_x = B_x = \beta_x = 0$. Vertical coherence is assumed to imply that β_z is significantly small in comparison with A_z/A and likewise φ'_z is of small magnitude in comparison with φ'_x. Hence,

$$x'_x = A\varphi'_x\cos\varphi'; \quad x'_z = A_z\sin\varphi'; \quad \overline{x'_x x'_z} = A_z\overline{A\varphi'_x\sin\varphi'\cos\varphi'} \tag{2.7}$$

$$z'_x = B\varphi'_x\cos(\varphi' + \beta); \quad z'_z = B_z\sin(\varphi' + \beta); \tag{2.8}$$

$$\overline{z'z'} = B_z\overline{B\varphi'_x\sin(\varphi' + \beta)\cos(\varphi' + \beta)}\,.$$

However,

$$\varphi'_x\sin\varphi'\cos\varphi' = \frac{1}{4}(\sin 2\varphi')_x; \tag{2.9}$$

$$\varphi'_x\sin(\varphi' + \beta)\cos(\varphi' + \beta) = \frac{1}{4}[\sin 2(\varphi' + \beta)]_x$$

and the Reynolds average of these quantities equals zero, which agrees with (2.4).

If the "non-intermittancy" requirement (2.4) is satisfied, the eddy fluxes (1.7) and (1.8) in horizontally homogeneous states are simplified as follows:

$$(2.10)\quad -\overline{w'u} = \overline{x'z'}\,\bar{u}_z\bar{u}_z - (\overline{x'_z z'} - \overline{z'_z x'})\,\bar{u}_z\,\overline{u-u_{ref}} - (\overline{x'_z z'_z} - \overline{x'_x z'_x})\,\overline{(u-u_{ref})^2},$$

$$(2.11)\quad -\overline{w's} = \overline{x'z'}\,\bar{u}_z\bar{s}_z - \overline{x'_z z'}\,\bar{s}_z\,\overline{u-u_{ref}} + \overline{z'_z x'}\,\bar{u}_z\,\overline{s-s_{ref}} - (\overline{x'_z z'_z} - \overline{x'_x z'_x})\,\overline{u-u_{ref}}\;\overline{s-s_{ref}}.$$

The corresponding forms for K(u) and K(s) can readily be derived and need not be written down. Obviously, the first two steps towards simplification do not yet achieve strictly gradient diffusion nor do they guarantee equality of eddy diffusivities.

The phenomenon of intermittancy in turbulence structure was first described by Corrsin (1943). It refers to the observational fact that the time-series (fluctuation recordings) of various turbulent variables may show a certain level of turbulence intensity for limited periods of time only, alternated by significantly lower turbulence levels (or nearly calm conditions) for interspersed comparable periods of time. Yih (1969) states that intermittancy, while first discovered in the outer regions of boundary layers, has later been found to penetrate deeply towards the boundary. According to Yih (1969) this "spotty structure" of turbulence may occur in relation to "convergent parts of the flow." This is interesting insofar as the "non-intermittancy" requirement (2.4) is actually, at least in part, based on the divergence terms of the eddy displacement vector; see (1.2). Certain implications of a failure to satisfy the "non-intermittancy" requirement will be briefly discussed in Section 3. Also, it will be demonstrated elsewhere that it is "intermittancy" which dominates eddy structure in airflow below the canopy of a forest (or other plant communities) and likewise in airflow below roof-top level of a city, that is the part of the boundary layer occupied by buildings acting as roughness elements of atmospheric flow.

2.3 Karman Similarity of Eddy Displacements

Equations (2.1) and (2.4) evidence that the first two steps towards simplification of eddy fluxes involved the longitudinal length-scales and their derivatives. The next step and two more which follow involve the covariances $\overline{x'z'}$. This term represents the "lateral length-scale," according to Lettau (1966). Firstly, consider the covariances which are parts of the second derivative, $(\overline{x'z'})_{zz}$. A boundary value of this term had previously been identified as the eddy-structure expression of the Karman constant; see also Section 2.5. In view of this it is assumed that the eddy displacement components x' and z' satisfy the requirement of "Karman similarity" if

$$\overline{x'_z z'_z} = \overline{x'_x z'_x} \neq 0 . \tag{2.12}$$

When "Karman similarity" exists in addition to horizontal homogeneity and vertical coherence, the eddy fluxes (1.7) and (1.8) are simplified as follows,

$$-\overline{w'u} = \overline{x'z'}\,\bar{u}_z\bar{u}_z - (\overline{x'_z z'} - \overline{z'_z x'})\,\bar{u}_z\,\overline{u-u_{ref}}\,, \tag{2.12)'}$$

$$-\overline{w's} = \overline{x'z'}\,\bar{u}_z\bar{s}_z - \overline{x'_z z'}\,\bar{s}_z\,\overline{u-u_{ref}} + \overline{z'_z x'}\,\bar{u}_z\,\overline{s-s_{ref}} . \tag{2.13}$$

The corresponding eddy diffusivities are

$$K(u) = \overline{x'z'}\,\bar{u}_z - (\overline{x'_z z'} - \overline{z'_z x'})\,\overline{u-u_{ref}}\,, \tag{2.14}$$

$$K(s) = \overline{x'z'}\,\bar{u}_z - \overline{x'_z z'}\,\overline{u-u_{ref}} + \overline{z'_z x'}\,\bar{u}_z\,\overline{s-s_{ref}}/\bar{s}_z . \tag{2.15}$$

When the convenient abbreviation $S = \bar{u}_z\,\overline{s-s_{ref}}/\bar{s}_z\,\overline{u-u_{ref}}$ is introduced, (2.15) can be restated with the aid of (2.14) as follows,

$$K(s) = K(u) - \overline{z'_z x'}\,\overline{u-u_{ref}}(1 - S). \tag{2.16}$$

Interestingly, Karman similarity of eddy structure, in addition to horizontal homogeneity and non-intermittancy, is necessary and sufficient to achieve gradient diffusion but only for momentum. The eddy diffusivity for admixture will equal that for momentum when there is perfect degree of mean profile similarity, that is $S = 1$ in (2.16). However, it should be noted that even for strictly gradient type momentum diffusion there is no guarantee that $K(u)$ in Eq. (2.14) must always be positive.

2.4 Prandtl Symmetry of Eddy Displacements

It is proposed to speak of Prandtl symmetry if the following requirement is satisfied,

$$\overline{x'_z z'} = \overline{z'_z x'} . \tag{2.17}$$

This nomenclature is explained by the fact that introduction of (2.17) into (2.12) and (2.13) produces the equivalent of the "classical" Prandtl-formula of eddy flux of momentum, namely, with ℓ = "mixing length" $= \overline{x'z'}^{1/2}$

(2.18) $$-\overline{w'u} = \overline{x'z'}\,\bar{u}_z\bar{u}_z , \quad = (\ell)^2\,(\bar{u}_z)^2 ,$$

while the eddy flux of admixture is still more complicated than Prandtl's form, namely,

(2.19) $$-\overline{w's} = \overline{x'z'}\,\bar{u}_z\bar{s}_z - \overline{z'_z x'}\,(\bar{s}_z\,\overline{u-u}_{ref} - \bar{u}_z\,\overline{s-s}_{ref}) .$$

The corresponding eddy diffusivities are

(2.20) $$K(u) = \overline{x'z'}\,\bar{u}_z = \ell^2\,u_z ,$$

(2.21) $$K(s) = K(u) - \overline{z'_z x'}\,\overline{u-u}_{ref}(1 - S).$$

The interesting consequence is that in view of (2.20), eddy diffusivity for momentum must be zero in a flow region with vanishing mean shear, while (2.21) shows that simultaneously, as long as $\overline{s-s}_{ref}/s_z\,\overline{u-u}_{ref}$ remains finite (which means $S = 0$ for $\bar{u}_z = 0$), the eddy diffusivity $K(s)$ can be finite. This may suggest that if Prandtl-symmetry exists, it is restricted to zones of uniform mean shear. Further remarks will be added in Section 3.

2.5 Universality of the Karman Constant

The final step in the sequence of model simplifications is the requirement that

(2.22) $$\overline{x'_z z'_z} = k^2 = \text{universal constant} = \text{Karman constant.}$$

Namely, if (2.17) is valid, another differentiation with respect to z yields

(2.23) $$\overline{x'_{zz}z'} + \overline{x'_z z'_z} = \overline{z'_{zz}z'_z} + \overline{z'_z x'_z} \;;\; \text{or,} \quad \overline{x'_{zz}z'} = \overline{z'_{zz}x'} .$$

On the other hand, the mixing length of turbulent shear flow, ℓ, according to Prandtl's model, is a strictly linear function of distance from the boundary which implies that $\ell_z = \text{const} = k$, and $\ell_{zz} = 0$. Hence $(\ell^2)_{zz} = 2k^2$. As noted before, Lettau (1964,67) and has shown that $\overline{x'z'} = \ell^2$. Hence, with the aid of (2.23)

(2.24) $$(\overline{x'z'})_{zz} = 2\overline{x'_z z'_z} + 2\overline{x'_{zz}z'} = 2\overline{x'_z z'_z} + 2\overline{z'_{zz}x'} .$$

Thus, in eddy structure showing Prandtl symmetry, the universality of the Karman constant requires that $\overline{x'_{zz}z'} = \overline{z'_{zz}x'} = 0$.

The ultimate step towards simplification (2.22) in the hierarchy of eddy flux models which originated with Eqs. (1.7) and (1.8) yields,

$$(2.25) \quad -\overline{w'u} = (kz\,\bar{u}_z)^2; \text{ or, } (\log_e \bar{u})_z = (-\overline{w'u})^{1/2}/k\,,$$

$$(2.26) \quad -\overline{w's} = (kz)^2\,\bar{u}_z\bar{s}_z + k^2 z(\bar{u}_z\,\overline{s-s}_{ref} - \bar{s}_z\,\overline{u-u}_{ref})\,.$$

Equation (2.25) produces directly the logarithmic law of the mean wind profile but only if the momentum-flux-divergence is negligible (which is acceptable for surface layer conditions). However, even for momentum surface layer conditions, and a universally applicable mixing length, Eq. (2.26) shows readily that the structure of eddy flux of a scalar admixture differs from that of momentum flux. It is important to realize than no less than five discrete steps of specialization were necessary to develop the simplified versions (2.25) and (2.26) from (1.7) and (1.8). This suggests that extreme caution must be exercised in any use of the simplified system.

3. Conclusions

The developments in Section 2 show that the eddy flux of fluid property in an elementary type of turbulent flow is proportional to the respective mean gradient only if coherence (non-intermittancy) and Karman similarity are assumed. Horizontal (downstream) homogeneity of eddy structure and mean flow is not an essential prerequisite for gradient diffusion. Although momentum diffusion may be of the gradient type, it is possible and quite likely that the simultaneous process of admixture diffusion (in the same fluid region) may fail to be proportional to the gradient of mean admixture.

Correspondingly, the eddy diffusivities for momentum and admixture can show significant variances. It follows most readily with the aid of Eq. (2.16) that there are two prerequisites for K(s) being different from K(u), namely: (1) dissimilarity of mean profile structure, or $S \neq 1$, and (2) an existing covariance between downstream eddy displacements x' and the vertical derivative of vertical eddy displacements, z'_Z. It can be expected that $\overline{z'_Z z'_Z}$ as well as $\overline{z'z'}$ must be affected by buoyancy forces due to surface heating or cooling. Thus, conclusions based on effects of $\overline{z'_Z x'}$ may explain the observational fact that (for example, in micrometeorological surface layers over bare fields) momentum diffusivity may equal heat diffusivity only for close to adiabatic conditions, while with the onset of surface heating or cooling a significant dissimilarity between mean profiles of wind and temperature develops which appears to produce differences between eddy diffusivities.

Another important consequence of (2.14) and (2.15) is that eddy diffusivities can be finite in flow regions of vanishing mean shear, namely, when $\bar{u}_z = 0$, but $\bar{s}_z \neq 0$,

$$(3.1) \qquad K(u)(\text{for } \bar{u}_z = 0) = (\overline{z'_z x'} - \overline{x'_z z'})\,\overline{u-u_{ref}}$$

$$(3.2) \qquad K(s)(\text{for } \bar{u}_z = 0) = \overline{x'_z z'}\;\overline{u-u_{ref}} \quad .$$

These expressions will be valid in unidirectional flow produced by a constant pressure gradient in a fluid between two parallel plates, with cross-stream transfer of heat from one wall (maintained at relatively high temperature) towards the opposite (cooled) wall, as for example in the series of experiments originally reported by Page et al. (1952), and extensively analyzed by Chia and Sage (1970). Eddy diffusivities of heat and momentum appear to be close to each other only in the vicinity of the walls (where $(\overline{s-s_0}/\bar{s}_z = \bar{u}/\bar{u}_z$, and $z\bar{u}_z$ large in comparison with $\bar{u}$), while in the core region, including the center (where $\bar{u}_z = 0$) eddy diffusivity for momentum was conclusively proven to be still finite but systematically smaller (involving a factor of about 2/3) than eddy diffusivity for heat. Thus, Eq. (2.16) suggests that $\overline{z'_z x'} < 0$ in the core region of duct flow.

The defining equations (1.1) cannot produce meaningful results if the assumption of "non-intermittancy" is dropped for regions of vanishing mean shear. However, the eddy flux of momentum can remain finite. For example, when $\bar{u}_z < 0$, (2.2) and (2.3) yield the following:

$$(3.3) \qquad -\overline{w'u} = -(\overline{x'_x x'_z} - \overline{z'_x z'_z} + \overline{x'_z z'_z} - \overline{x'_x z'_x})(\overline{u-u_{ref}})^2 \,,$$

$$(3.4) \qquad -\overline{w's} = -\overline{x'_z z'}\;\bar{s}_z\;\overline{u-u_{ref}} + -(\overline{x'_x x'_z} - \overline{z'_x z'_z} + \overline{z'_z z'_z} - \overline{x'_x z'_x})\;\overline{u-u_{ref}}\;\overline{s-s_{ref}} \,.$$

Again, the mean profile of admixture may not be similar to that of momentum. An example for this type of flow is the upper tropospheric jet stream, for which "negative" eddy viscosity has been suggested, while meridional transfer of heat appears to follow the temperature gradient; reference is made to Starr (1968).

The purpose of this short note is merely to outline the problem of eddy diffusivities as seen from the viewpoint of a generalization of eddy structure concepts. It may be concluded that there are promising aspects for a more systematic and more detailed investigation.

4. References

Chia, Wu-sun, and B. H. Sage: "Temperature gradients in turbulent gas streams: Investigation of the limiting value of total Prandtl number," AI Ch E Journal, 16, pp. 37-43, 1970.

Corrsin, S.: "Investigation of flow in an axially symmetric heatet jet of air," Natl. Advis. Comm. Aeron., Advanced Rep. No. 3L23, 1943.

Lettau, H.: "A new vorticity-transfer hypothesis of turbulence theory," Journal Atm. Sciences, 21, pp. 453-456, 1964.

Lettau, H.: "Longitudinal versus lateral eddy length scale," Journal Atm. Sciences, 23, pp. 151-158, 1966.

Lettau, H.: "New hypothesis for the relationship between eddy and mean states," The Physics of Fluids, Supplement, pp. 79-83, 1967.

Page, F., W. H. Corcoran, W. G. Schlinger, and B. H. Sage: "Temperature gradients in turbulent gas streams," Industr. and Engineering Chemistry, 44, pp. 419-424, 1952.

Starr, V. P.: Physics of Negative Viscosity, McGraw-Hill Book Co., New York, 1968.

Yih, C.-S.: Fluid Mechanics, 622 pp., McGraw-Hill Book Company, New York, 1969.

Scanner's note:

This page is blank.

CONVERSION OF PROFILE DIFFERENCE QUOTIENTS TO TRUE GRADIENTS AT THE GEOMETRIC MEAN HEIGHT IN THE SURFACE LAYER*

Charles R. Stearns

ABSTRACT: Theoretical profiles of wind speed and air temperature can provide "synthetic measurements" at discrete levels which may be compared with actual field measurements. In addition to wind and temperature gradients at any height, profile theory permits us to determine the difference quotients from measurements at discrete levels. It is shown that corrections are required to obtain the gradients at the geometric mean height of the two discrete levels of measurement. The correction factor depends on the measurement height and spacing, profile structure, surface roughness and the measured Richardson number. The correction can be reduced by close spacing of the measurement levels.

1. Introduction

Profile measurements of wind speed and air temperature in the surface layer are used to study profile structure and determine the flux densities of sensible heat and momentum. Commonly, vertical spacing of measurement points is so chosen that $z_2 = 2z_1$ (double levels) where z_2 (cm) is next above z_1 (cm). Profile structure parameters and intensities of fluxes depend on the equivalence between true gradients and the difference quotient as determined from a wind or temperature difference between two levels divided by the height difference. The height at which the difference quotient is equal to the true gradient will depend upon profile structure.

Lettau (1957) has used the geometric mean height defined as $z_{12} = (z_1 \cdot z_2)^{1/2}$ for the height assignment of the difference quotient in wind and temperature. According to Dyer (1967) the underestimation of the true gradient by the difference quotient at the geometric mean height is 2% for double levels and 7.7% for fourfold height intervals ($z_2 = 4z_1$). Swinbank (1968) assigned gradient measurements to the logarithmic mean height which turned out to be 2.17 m for $z_1 = 1.00$ m and $z_2 = 4.00$ m. The geometric mean height of the two levels would be 2.00 m. Swinbank

*Accepted for publication in Boundary-Layer Meteorology, Vol. 1, No. 2, 1970.

corrected the height at which the difference quotient applied while Dyer corrected the difference quotient at the geometric mean height of the two measurement levels. Either correction requires an assumption about the profile structure before it can be evaluated.

The purpose of this paper is to show how the corrections will vary with the profile structure assumptions, the surface roughness, Richardson's number, and the height and spacing of the measurement levels. The method was to generate synthetic wind and temperature, then compare the difference quotients to the true gradients at the geometric mean height. The synthetic wind and temperature profiles were calculated under the assumption that the fluxes of heat and momentum were constant over the profile height.

2. Theory of Profile Structure in the Atmospheric Surface Layer

The synthetic wind and temperature profiles are based on the KEYPS model (Kazansky and Monin, 1956; Ellison, 1957; Yamamoto, 1959; Panofsky et al., 1960; Sellers, 1962) of profile structure with some modifications by Stearns (1968).

The Monin-Obukow (1954) non-dimensional wind shear or Lettau's (1962) diabatic influence function

$$\phi = k(z + z_0)V'V^{*-1} \tag{1}$$

where k = the von Karman constant (0.428), z = height (cm), z_0 = surface roughness (cm), V' = wind gradient (sec^{-1}) and V^* = friction velocity (cm sec^{-1}). The height coordinate system is chosen so that at $z = 0$ we have the boundary condition $\phi = 1$ and V' is finite.

Integration of (1) with respect to z gives

$$V(z) = V^* k^{-1}[\ln \frac{z + z_0}{z_0} + \Phi(z)] \tag{2}$$

where $\Phi(z) = \int_0^z (\phi - 1)(z + z_0)^{-1} dz$ is the integral diabatic influence function defined by Lettau (1962).

The modification of the KEYPS model by Stearns (1967) is expressed as

$$\phi K_h K_m^{-1} Ri = -(z + z_0) L^{-1} \tag{3}$$

where K_h = eddy diffusivity for heat ($cm^2\ sec^{-1}$) and K_m = eddy diffusivity for momentum ($cm^2\ sec^{-1}$). The Richardson number (Ri) is defined as

$$Ri = g\, T_m^{-1} \theta' V'^{-2} \tag{4}$$

where g = acceleration of gravity ($cm\ sec^{-2}$), T_m = mean temperature of the air layer (K), and θ' = potential temperature gradient ($K\ cm^{-1}$). L is the LMO length scale of turbulence (Neumann, 1964) defined as $L = g^{-1} k^{-1} \rho\, c_p\, T_m\, Q_0^{-1} V^{*3}$ where c_p = specific heat of air at constant pressure ($cal\ g^{-1}\ K^{-1}$), ρ = air density ($g\ cm^{-3}$), and Q_0 = sensible heat flux ($cal\ cm^{-2}\ sec^{-1}$).

Solving (3) and (4) for the potential temperature gradient, one obtains

$$\theta' = - T^* K_m K_h^{-1} \phi (z + z_0)^{-1} \tag{5}$$

where $T^* = k^{-1} \rho^{-1} c_p^{-1} Q_0 V^{*-1}$ (deg K). At $z = 0$, θ', V' and Ri are finite. The diffusivities K_h and K_m are defined as

$$K_h = - k T^* V^* \theta'^{-1} \tag{6}$$

and

$$K_m = V^{*2} V'^{-1} . \tag{7}$$

Integration of (5) with respect to height yields

$$\theta(z) = \theta_0 - T^* [\ln \frac{z + z_0}{z_0} + \Phi_T(z)] \tag{8}$$

where θ_0 is the potential temperature (K) at $z = 0$, and $\Phi(z) = \int_0^z K_m K_h^{-1} (\phi - 1)(z + z_0)^{-1} dz$ is the integral diabatic influence function for the temperature profile (Stearns, 1967, 1968). If $K_h = K_m$ then $\Phi_T = \Phi$ and the wind and temperature profiles are similar. An alternate assumption considered here is that $K_h K_m^{-1} = \phi^{-1/2}$ (Stearns, 1967) as an example of wind and temperature profiles which are not similar.

The KEYPS model gives the relationship between ϕ and $(z + z_0)L^{-1}$ as

$$\phi(1 - \phi^{-4})/18 = - (z + z_0)L^{-1} \tag{9}$$

which is used to obtain ϕ given $z + z_0$ and L (Stearns, 1969).

Shape factors for profile structure (Lettau, 1962) are the Deacon numbers defined as

$$DEU = - d \ln V'/d \ln(z + z_0) \tag{10}$$

for the wind profile and

$$DET = - d \ln \theta'/d \ln(z + z_0) \tag{11}$$

for the temperature profile. Theoretical values at a given height depend on ϕ (Stearns, 1967) as

$$DEU = 4\phi^{-4}(1 + 3\phi^{-4})^{-1} . \tag{12}$$

DET = DEU for $K_h = K_m$, and

$$DET = 1.5\ DEU - 0.5$$

if $K_h K_m^{-1} = \phi^{-1/2}$. (13)

3. Procedure

The synthetic wind and temperature profiles were calculated using values of $\theta_0 = 273.16$K, P = 1000 mb, g = 980 cm sec^{-2}, $z_0 = 0.05$ or 1.0 cm, with V^* and T^* changed systematically to vary L^{-1}. ϕ is determined from the assigned value of $z + z_0$ by (9). The discrete levels were chosen as $z_{i+1} = nz_i$ where i is an index increasing with height, $z_i = 5.0$ cm for i = 1, while n was chosen either as $\sqrt{2}$, 2 or 4. Φ and Φ_T were determined from ϕ (Stearns, 1969). Using V^* and z_0, the wind speed was computed at $z_i + z_0$ using (2) and the potential temperature by (8) with either one of the two assumptions about $K_h K_m^{-1}$.

Given $V(z_2)$, $V(z_1)$ and $\theta(z_2)$, $\theta(z_1)$, the difference quotients V_m' for wind and θ_m' for temperature were calculated as

$$V_m'(z_{12} + z_0) = [V(z_2 + z_0) - V(z_1 + z_0)]/[z_2 - z_1] \tag{14}$$

$$\theta_m'(z_{12} + z_0) = [\theta(z_2 + z_0) - \theta(z_1 + z_0)]/[z_2 - z_1]. \tag{15}$$

The true gradients V_T' and θ_T' at the geometric mean height of the two levels $z_{12} = (z_1 z_2)^{1/2}$ were determined from (1) and (5), respectively. The ratios of V_T'/V_m' and θ_T'/θ_m' were calculated to obtain the correc-

tion.factor. The measured Deacon numbers DEU_m for wind and DET_m for temperature were determined as

$$DEU_m = - d \ln V_m'/d \ln(z_{12} + z_0) \quad (16a)$$

$$DET_m = - d \ln \theta_m'/d \ln(z_{12} + z_0) . \quad (16b)$$

The true values of DEU_T, DET_T were determined by (12) and (13) where ϕ is determined from (9) at $z_{13} = (z_{12}' z_{23})^{1/2}$ the geometric mean of the heights assigned to V_m' and θ_m'.

Richardson numbers were calculated for comparison with Deacon numbers. They were assigned the geometric mean height of the Deacon numbers z_{13} and were determined from the following equation.

$$Ri_m = \frac{g[\theta(z_3 + z_0) - \theta(z_1 + z_0)][z_3 - z_1]}{T_m[V(z_3 + z_0) - V(z_1 + z_0)]^2} . \quad (17)$$

4. Results

Consider the adiabatic case where $\theta' = 0$. Let $z_2 = nz$, then $z_{12} = z_1\sqrt{n}$ where n = alternately $\sqrt{2}$, 2, or 4.

From (1) we have that

$$V_T' = V^* k^{-1}(z_{12} + z_0)^{-1} \quad (18)$$

and from (14) that

$$V_m' = \frac{V^* k \ln(\frac{z_2 + z_0}{z_1 + z_0})}{z_2 - z_1} . \quad (19)$$

Then

$$V_T'/V_m' = \frac{(z_2 - z_1)}{(z_{12} + z_0) \ln(\frac{z_2 + z_0}{z_1 + z_0})} . \quad (20)$$

The height z where $V_T'/V_m' = 1$ follows as

$$z + z_0 = (z_2 - z_1)/\ln(\frac{z_2 + z_0}{z_1 + z_0}) . \quad (21)$$

The correction factor for the measured value V_m' assigned to the height z_{12} as obtained from (20) depends on z_0, z_2 and z_1. Table I illustrates the ratio V_T'/V_m' for several height arrangements, employing $z_0 = 0.05$ and 1.0 cm. Swinbank's height of 2.17 m for the difference quotient corresponds to $n = 4$ in Table I which, when applied to $z_1 = 1.0$ m and $z_2 = 2.0$ m, gives $2.17/2.0 = 1.085$. Dyer's estimate of 2% error for $n = 2$ is confirmed, but his 7.7% error for $n = 4$ does not agree with either Swinbank or Table I. The correction factors in Table I remain within 1% for $z_0 = 1.0$ cm. Interestingly, when $n = \sqrt{2}$ the required correction factor on V' is negligibly small for the selected profile structure which illustrates the importance of closely spaced measurement levels.

Table I. The ratio V'_T/V'_m for $z_0 = 1.0$ and 0.05 cm for geometric height intervals where z_2 (cm) $= nz_1$ (cm). The height variation reflects the dependence of the ratio on z_0.

	V'_T/V'_m					
	$z_0 = 1.0$			$z_0 = 0.05$ cm		
n	$z_1 = 5.0$	$5.0\,n$	$5.0\,n^2$	5.0	$5.0\,n$	$5.0\,n^2$
$\sqrt{2}$	1.006	1.005	1.005	1.005	1.005	1.005
2	1.022	1.021	1.021	1.020	1.020	1.020
4	1.089	1.084	1.083	1.082	1.082	1.082

The correction required to obtain the true gradient at the geometric mean height of the measurement levels varies systematically with Ri_m, as illustrated in Figure 1 for lapse conditions ($Ri_m < 0$). The dependence of the correction factor on height is not shown but is similar to the results in Table I as Ri_m varies. Plots of θ'_T/θ'_m or V'_T/V'_m versus θ'_m or V'_m do not show a continuous variation in the correction factor.

Table I yields an error of less than 1% for $Ri_m < 0$. The assumption that $K_h K_m^{-1} = \phi^{-1/2}$ alters the results in Figure 1 by less than 1%, which is considered insignificant.

During inversion conditions ($Ri_m > 0$) the correction factor does not behave as nicely as for lapse conditions. Figure 2 shows the correction factor as a function of Ri_m exemplified by the case for $K_h K_m^{-1} = \phi^{-1/2}$. The correction factors for the adiabatic profile hold to within approximately 1% out to $Ri_m = 0.01$. This would be satisfactory for most purposes.

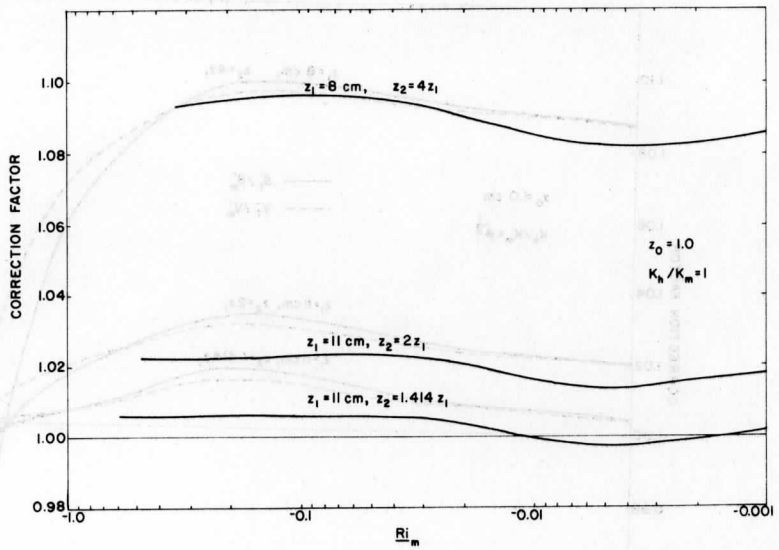

Fig. 1. The correction factor required to obtain the true gradient from the difference quotient of wind and temperature at the geometric mean height as a function of Ri_m for $Ri_m < 0$. The levels used are $z_2 = nz$, where $n = \sqrt{2}$, 2 or 4. Since $K_h = K_m$, the same correction factor applies to both the wind and temperature difference quotients.

The corrected difference quotients may also be used for determining the heat and momentum flux or determining Ri and L^{-1} from (3) (Stearns, 1969).

The gradients V'_T and θ'_T at the geometric mean height of the two measurement levels can be calculated from

$$V'_T(z_{12} + z_0) = \frac{[V'_m[z_2 - z_1]}{[z_{12} + z_0][\ln \frac{z_2 + z_0}{z_1 + z_0} + \Phi(z_2) - \Phi(z_1)]} \qquad (22)$$

and

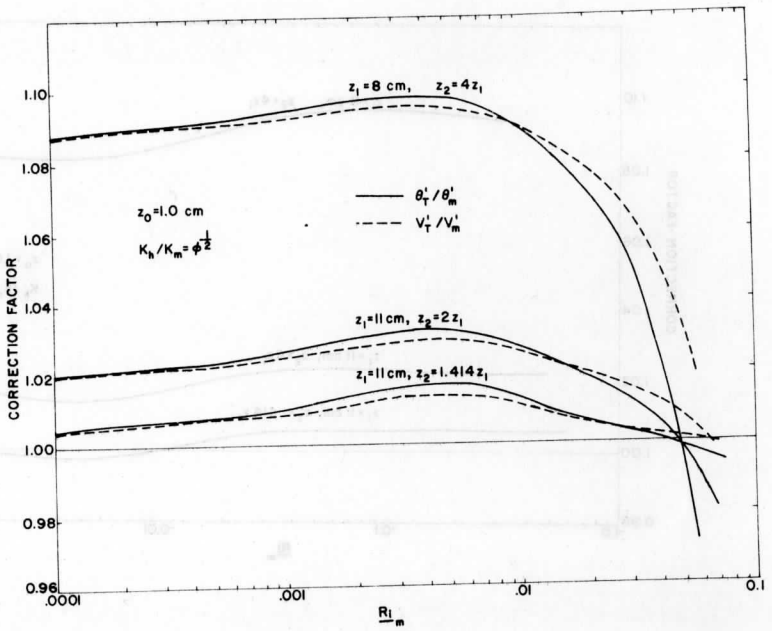

Fig. 2. The correction factor required to obtain the true gradient from the difference quotient of wind and temperature at the geometric mean height as a function of Ri_m for $Ri_m > 0$. The levels used are $z_2 = nz$, where $n = \sqrt{2}$, 2, or 4. $K_h K_m^{-1} = \sigma^{-1/2}$; therefore the wind and temperature difference quotients do not have the same correction factor at the same Ri_m.

$$\theta'_T(z_{12} + z_0) = \frac{\theta'_m[z_2 - z_1]}{[z_{12} + z_0]\left[\ln \frac{z_2 + z_0}{z_1 + z_0} + \Phi_T(z_2) - \Phi_T(z_1)\right]} . \quad (23)$$

Ri calculated from the corrected difference quotients will be correct for the assumed profile structure.

The error in DEU and DET was checked but found to be insignificant. When using a geometric spacing, Figure 3 shows the theoretical value of DEU_T and DET_T vs. Ri_T and the results obtained by using the measured values of DEU_m and DET_m vs. Ri_m for inversion conditions. It should be remembered that three measurement levels are required for calculating DEU_m and DET_m while only the two extreme levels are used for determining Ri_m. The error is not significant for lapse conditions using a geometric spacing of levels.

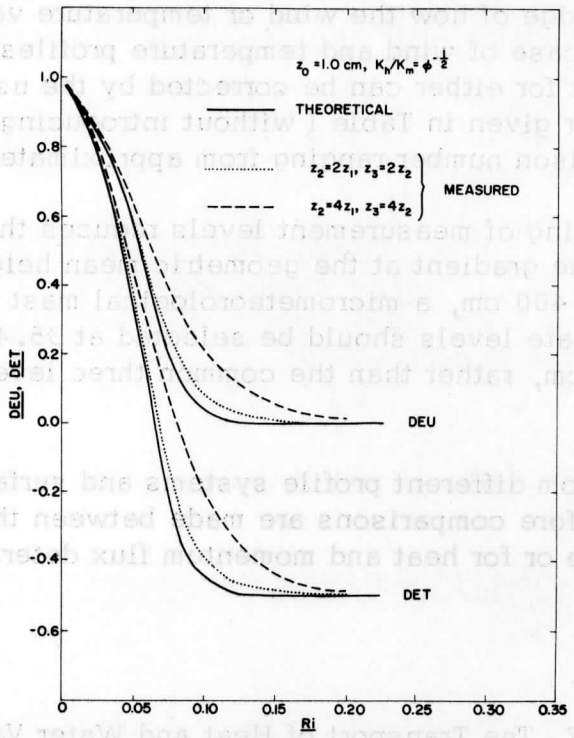

Fig. 3. Deacon number for wind (DEU) and for temperature (DET) as a function of Ri. The profile structure results are influenced by the instrument spacing.

The Deacon numbers can be assigned to the same geometric height as the Richardson number only for a geometric spacing of the measurement levels. Thus the geometric height of Ri_m is $z_{13} = (z_1 \cdot z_3)^{1/2}$, while that for the Deacon numbers is $z_{123} = (z_{12} \cdot z_{23})^{1/2}$. For $z_{13} = z_{123}$ we have that $(z_1 \cdot z_3)^2 = z_1 \cdot z_2^2 \cdot z_3$ but this is only true when a geometric spacing of measurement levels is used. A linear spacing of levels will result in a geometric height for Deacon numbers which differs from that for the Richardson number.

It is apparent from Figure 3 that the selected levels will influence the theoretical results significantly except for the case where $z_2 = \sqrt{2}z_1$. This relationship is not illustrated in Figure 3 because the departure from the theoretical curve was not apparent.

5. Conclusions

Equating the difference quotient to the gradient at a given height requires a knowledge of how the wind or temperature varies between the two points. In the case of wind and temperature profiles, the value of the difference quotient for either can be corrected by the use of the adiabatic correction factor given in Table I without introducing an error larger than 1% for a Richardson number ranging from approximately -1.0 to +0.01.

Close spacing of measurement levels reduces the correction required to obtain the true gradient at the geometric mean height. If, for example, between 25 and 400 cm, a micrometeorological mast is to be instrumented, seven intermediate levels should be selected at 35.4, 50.0, 70.7, 100, 141, 200, 282 cm, rather than the common three levels at 50, 100, and 200 cm.

The data from different profile systems and surface roughnesses should be corrected before comparisons are made between the systems either for profile structure or for heat and momentum flux determinations.

6. References

Dyer, A. J.: 1967, The Transport of Heat and Water Vapor in an Unstable Atmosphere," Quart. J. Roy. Meteor. Soc. 93, 501-8.

Ellison, T. H.: 1957, Turbulent Transfer of Heat and Momentum from an Infinite Rough Plate, J. Fluid Mech. 2, 456-66.

Kazansky, A. B. and Monin, A. S. · 1956, Turbulence in the Inversion Layer near the Surface, Acad. Nauk. SSSR. Ser. Geophys. No. 1, pp. 79-86.

Lettau, H. H.: 1957, Computation of Richardson's Numbers Classification of Wind Profiles and Determination of Roughness Parameters, Exploring the Atmosphere's First Mile, Vol. I (ed. by Lettau and Davidson), Pergamon Press, New York and London, pp. 337-72.

Lettau, H. H.: 1962, Notes on Theoretical Models of Profile Structure in the Diabatic Surface Layer, Final Report, Contract DA-36-039-SE-80282, USAEPG, Fort Huachuca, Arizona, Univ. of Wisconsin, pp. 105-226.

Monin, A. S. and Obukhov, A. M.: 1954, Dimensionless Characteristics of Turbulence in the Surface Layer, Akad. Nauk. SSSR. Geofis. Trudy, No. 24, pp. 151-63.

Neumann, J. · 1964, Turbulent, Convection of Turbulent Kinetic Energy in Stratified Shear Flows, Sixth Annual Conference on Aviation and Astronautics, Feb. 1964, Tel Aviv and Haifa, Israel, pp. 47-9.

Panofsky, H. A., Blackadar, K., and McVehil, G. E.: 1960, The Diabatic Wind Profile, Quart. J. Roy. Meteor. Soc. 86, 390-98.

Sellers, W. D.: 1962, Simplified Derivation of the Diabatic Wind Profile, J. Atmos. Sci. 19, 180-81.

Stearns, C. R.: 1967, Micrometeorological Studies in the Coastal Desert of Southern Peru, Ph. D. Thesis, Dept. of Meteor., University of Wisconsin.

Stearns, C. R.: 1968, Analysis of Diabatic Wind and Temperature Profiles, Annual Report, Grant No. DA-AMC-28-043-66-G24, ECOM, Fort Huachuca, Arizona, Univ. of Wisconsin, pp. 1-56.

Stearns, C. R. 1969, The Determination of the Surface Roughness from Wind Speed and Air Temperature Profiles in the Surface Layer, Final Report, Grant No. DA-AMC-28-043-66-G24, ECOM, Fort Huachuca, Arizona, Univ. of Wisconsin, pp. 131-48.

Swinbank, W. C.: 1968, A Comparison Between Predictions of Dimensional Analysis for the Constant Flux Layer and Observations in Unstable Conditions, Quart. J. Roy. Meteor. Soc. 94, 460-67.

Yamamoto, G.: 1959, Theory of Turbulent Transfer in Non-Neutral Conditions, J. Meteor. Soc. Japan 37, 60-70.

Scanner's note:

This page is blank.

3

THE EFFECT OF TIME-VARIABLE FLUXES ON MEAN WIND AND TEMPERATURE PROFILE STRUCTURE

Charles R. Stearns

ABSTRACT: Synthetic wind speed and air temperature profiles based on the sensible heat flux density and stress at the surface are averaged for the four possible ways in which the surface stress and heat flux density can vary maintaining the same average values. The analysis of the averaged wind and temperature profiles shows that, when the surface stress and/or heat flux density are time-variable, and wind speed and air temperature are averaged linearly, an erroneous estimate of surface roughness, surface stress, heat flux density and profile structure parameters will result.

1. Introduction

Mean profile measurements of wind speed and air temperature near the earth's surface are often used to study profile structure and to estimate the flux densities of momentum and sensible heat. The measurements usually consist of the wind speed and air temperature at several vertically spaced levels above the surface averaged linearly for ten to thirty minutes or more. During the averaging time the surface values of heat flux density and stress may be changing. The resulting mean wind and temperature measurements do not necessarily represent the equilibrium profile for the average stress and heat flux density.

The purpose of this paper is to show that, for profile measurement averaging times during which the fluxes of heat and momentum are varying, the analysis of the mean wind and temperature profile will not yield the mean fluxes. The measured profile structure will be different from the equilibrium profile structure for the mean surface fluxes.

2. Synthetic Profiles

Synthetic wind speed and air temperature profiles were computer generated following the method used by Stearns (1970a). The profiles are in equilibrium with a surface roughness of 1.0 cm which corresponds to mowed grass. Table 1 gives the values of temperature and wind generated

Table 1. Surface stress (τ_0, dynes cm^{-2}) and sensible heat flux density (Q_0, ly min^{-1}) used to obtain the LMO (L, cm) length scale of turbulence from which wind speed (V, cm sec^{-1}) and potential air temperature (θ, deg K) were computed at selected heights.

τ_0	Q_0	θ_{20}	θ_{320}	V_{20}	V_{320}	1/L
0.500	0.100	-1.867	-3.209	134.4	231.0	1.07×10^{-3}
	0.200	-3.633	-5.750	130.8	214.2	2.15×10^{-3}
	0.300	-5.314	-8.455	127.5	202.9	3.22×10^{-3}
1.00	0.100	-1.344	-2.451	193.5	353.0	3.80×10^{-4}
	0.200	-2.662	-4.678	191.6	336.8	7.59×10^{-4}
	0.300	-3.953	-6.768	189.7	324.9	1.14×10^{-3}
1.500	0.100	-1.101	-2.058	237.8	444.6	2.07×10^{-4}
	0.200	-2.192	-3.984	236.8	430.2	4.13×10^{-4}
	0.300	-3.272	-5.819	236.6	419.0	6.20×10^{-4}
0.500	-0.025	0.486	1.071	139.5	293.0	-2.68×10^{-4}
	-0.050	0.975	2.333	140.4	336.0	-5.37×10^{-4}
	-0.075	1.492	5.384	141.5	389.7	-8.05×10^{-4}
1.000	-0.025	0.343	0.683	196.7	388.5	-0.49×10^{-5}
	-0.050	0.686	1.438	197.0	401.3	-1.90×10^{-4}
	-0.075	1.032	2.301	197.3	417.3	-2.85×10^{-4}
1.500	-0.025	0.280	0.547	240.8	469.9	-5.17×10^{-5}
	-0.050	0.559	1.121	240.9	477.1	-1.03×10^{-4}
	-0.075	0.840	1.726	241.1	485.3	-1.55×10^{-4}

θ_{20} and θ_{320} are converted to deg C by subtracting 273.15K, the assumed temperature at z = 0.0 cm.

V_{20} and V_{320} are in cm sec^{-1}. The subscript refers to the nominal height in cm.

at 20 and 320 cm so that the variability of the wind speed and air temperature for the several assumed flux values may be apparent.

The profiles were computed using a potential temperature = 273.15 K at $z = 0$, surface pressure = 1000 mb, acceleration of gravity = 980 cm sec^{-2}, and specific heat of air = 0.24 cal $gm^{-1}K^{-1}$. The wind profile equation was

$$V(z) = V^{*}k^{-1}[\ln \frac{z + z_0}{z_0} + \Phi(z)] \qquad (1)$$

where $V(z)$ = wind speed (cm sec^{-1}) at the height z(cm), $k = 0.428$ the Karman constant, $V^{*} = (\tau_0/\rho)^{1/2}$ = friction velocity (cm sec^{-1}), where τ_0 = surface stress (dynes cm^{-2}) and ρ = air density (gm cm^{-3}). Φ is the integral diabatic influence function for wind (Lettau, 1962; Stearns, 1970a). The potential temperature profile equation is

$$\theta(z) = \theta_0 - T^{*}[\ln (\frac{z + z_0}{z_0}) + \Phi_T(z)] \qquad (2)$$

where $\theta(z)$ = the potential temperature (deg K) at the height z, θ_0 = the potential temperature at $z = 0$. $T^{*} = k^{-1} \rho c_p Q_0 V^{*-1}$ where c_p = the specific heat of dry air at constant pressure and Q_0 = sensible heat flux density (ly sec^{-1}). Φ_T is the integral diabatic influence function for the temperature profile (Stearns, 1970a).

The theoretical background for (1) and (2) are given in sufficient detail by Stearns (1970a, b). The synthetic profiles for lapse conditions ($Q_0 > 0$) assume the eddy diffusivities for heat (K_h, cm^2 sec^{-1}) and momentum (K_m, cm^2 sec^{-1}) are equal. The inversion profiles ($Q_0 < 0$) assume that the $K_h/K_m = \phi^{-1/2}$ where ϕ is Lettau's (1962) diabatic influence function (Stearns, 1970a).

The profile wind and temperature were averaged for four possible variations in Q_0 and τ_0. The average value of Q_0 was 0.200 ly min^{-1} for lapse and -0.050 ly min^{-1} for inversion, τ_0 always was 1.0 dynes cm^{-2}.

Table 2 identifies the five cases and gives the values of τ_0 and Q_0 used to obtain the mean wind speed and air temperature for each of the above cases. Case I was the original generated synthetic profile and served as a test case for the analysis method. The linear averaging is equivalent to having each of the extreme profiles measured for 50% of the recording period.

Table 2. Surface stress (τ_0 , dynes cm^{-2}) and sensible heat flux densities (Q_0 , ly min^{-1}) used to generate synthetic profiles which were then averaged to obtain profiles which could occur for the same surface average of τ_0 and Q_0 .

Case		Lapse		Inversion		
I	τ_0	1.0		1.0		constant
	Q_0	0.20		-0.05		constant
II	τ_0	1.0	1.0	1.0	1.0	constant
	Q_0	0.10	0.30	-0.025	-0.075	varying
III	τ_0	1.5	0.5	1.5	0.5	decreasing
	Q_0	0.10	0.30	-0.025	-0.075	increasing
IV	τ_0	1.5	0.5	1.5	0.5	varying
	Q_0	0.20	0.20	-0.05	-0.05	constant
V	τ_0	1.5	0.5	1.5	0.5	decreasing
	Q_0	0.30	0.10	-0.75	-0.025	decreasing

3. Profile Analysis

The wind and temperature profiles for the two sets of five cases were analyzed using the method described by Stearns (1970a). The profile structure assumptions used in the analysis method were exactly those used to generate the synthetic profiles.

The results are presented in Table 3. Case I was compatible with the assumptions used and the tolerance of 0.001 cm allowed in the determination of surface roughness (z_0 , cm) and 0.01 cm for displacement height (d, cm). The analysis method is the same for all profiles and is not biased by independent ideas of what the answers should be. The results assuming z_0 = 1.00 cm and d = 0.0 do not represent an improvement.

The poorest conditions are obviously Case III where high wind stress with low heat flux density is combined with low wind stress and high flux density. This is also the least likely of the set to occur in the surface

Table 3. Results of profile analysis for the five cases of synthetic wind and temperature profiles. Case I serves as a test of the analysis method. The average surface stress (τ_0) is 1.000 dyne cm^{-2}, the surface sensible heat flux density (Q_0) average is 0.200 ly min^{-1} for lapse and -0.050 ly min^{-1} for inversion for all cases. The surface roughness (z_0, cm), surface stress (τ dynes cm^{-2}), sensible heat flux (Q, ly min^{-1}) and the inverse of the LMO length scale of turbulence (1/L, cm^{-1}) determined by the aerodynamic method are given for lapse and inversion conditions for each case. The surface value of 1/L is 7.60×10^{-4} cm^{-1} for lapse and -1.90×10^{-4} cm^{-1} for inversion conditions. The second set of values for τ, Q and 1/L were determined using z_0 = 1.0 cm and d = 0.0 cm.

Case	I	II	III	IV	V
Lapse					
z_0	1.000	1.072	1.337	1.109	1.033
d	-0.001	0.451	2.197	0.813	0.202
τ	1.000	1.029	1.036	0,964	0.947
	1.000	1.000	0.915	0.934	0.924
Q	0.199	0.196	0.215	0.205	0.189
	0.199	0.192	0.194	0.187	0.197
$1/L \times 10^{-4}$	7.59	7.15	7.70	8.22	7.80
	7.59	7.01	8.04	7.83	8.34
Inversion					
z_0	1.002	1.013	1.340	1.035	1.515
d	0.024	0.159	2.517	0.280	3.392
τ	1.000	1.004	1.047	0.946	1.111
	1.000	1.000	0.936	0.934	0.943
Q	-0.050	-0.052	-0.101	-0.047	-0.026
	-0.050	-0.052	-0.091	-0.046	-0.065
$1/L \times 10^{-4}$	-1.90	-2.00	-3.83	-1.96	-2.46
	-1.90	-2.00	-3.97	-1.97	-2.61

layer but has been observed about sunrise at La Joya, Peru where the sensible heat flux density is increasing and the nighttime katabatic wind speed is decreasing (Stearns, 1969).

The most likely to be observed is Case IV where the sensible heat flux density is constant over the averaging time but the wind speed or stress varies as presented in Table 1. These are realistic changes in wind speed over time periods of a few minutes and are easily exceeded under even what are often considered steady conditions. The error in estimating τ_0 is larger than would be expected considering that instrumental error is not allowed.

The measured Richardson number (Ri) defined as

$$\underline{Ri} = g\, T_m^{-1}\, \theta' V'^{-2} \tag{3}$$

where T_m = mean temperature of the profile (deg K), θ' is the difference quotient for temperature and V' is the difference quotient for wind, is used to determine $1/L$ where $L = g^{-1} k^{-1}\, c_p\, T_m\, Q_0^{-1}\, V^{*3}$ (Stearns, 1970a). The measured Ri is partially corrected to the true value at the geometric mean height of the measurement levels to obtain $1/L$ (Stearns, 1970b). It is obvious from Table 3 that while the mean surface fluxes yield one value of $1/L$ only Case I agrees and the others are in error and the actual value of z_0 and d does not materially improve the results. Figure 1 illustrates the variations of Ri with height for each case.

In view of the discrepancies between LMO determined from the average surface fluxes and LMO determined from the wind and temperature profiles, it is suggested that the symbol L_0 refer to the value of LMO determined from average surface fluxes. L determined from profile measurements will not necessarily agree with the surface value L_0.

The Deacon number for wind defined as

$$\underline{DEU} = -\, d \ln V' / d \ln (z + z_0) \tag{4}$$

was calculated using the difference quotients determined from adjacent levels. Figures 2 and 3 present DEU as a function of height for lapse and inversion conditions respectively. Case I agrees with the theoretical value for both conditions. Figures 4 and 5 are similar presentations of the Deacon number for the temperature profile defined as

$$\underline{DET} = -\, d \ln \theta' / d \ln (z + z_0) \quad . \tag{5}$$

Figure 6 compares DET to DEU. Lettau (1962) has shown that

$$d \ln(K_h/K_m) \Big/ d \ln(z + z_0) = DET - DEU \, . \tag{6}$$

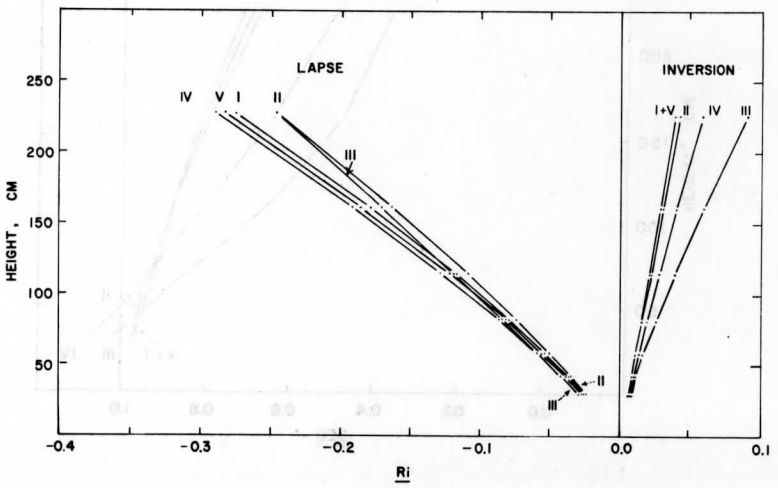

Fig. 1. Richardson number (Ri) as a function of height for lapse and inversion temperature structure.

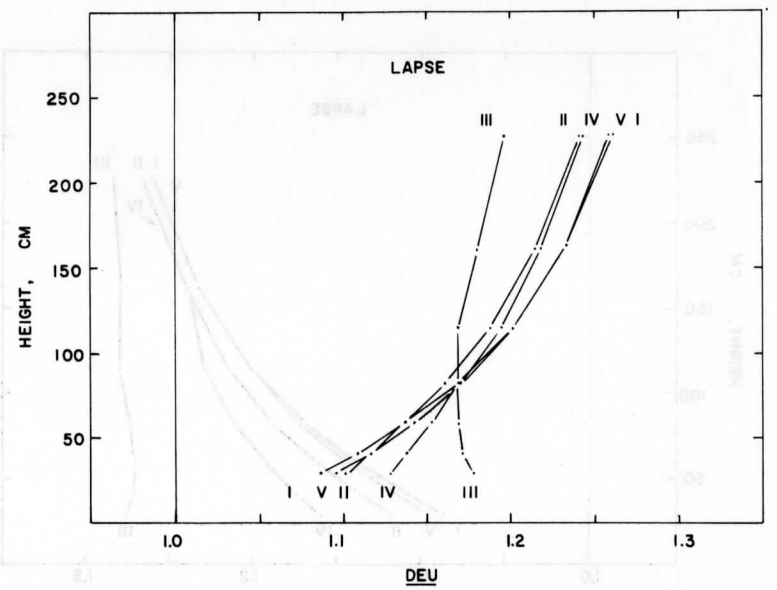

Fig. 2. Deacon number (DEU) as a function of height for lapse temperature structure.

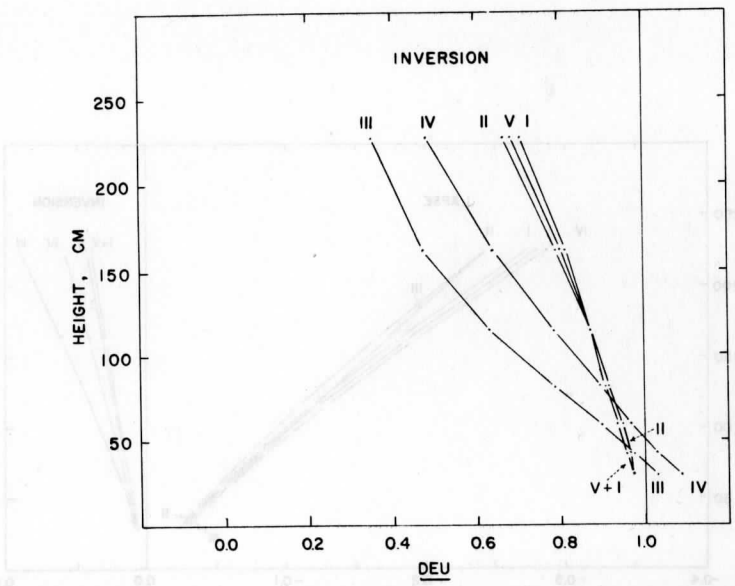

Fig. 3. Deacon number (DEU) as a function of height for inversion temperature structure.

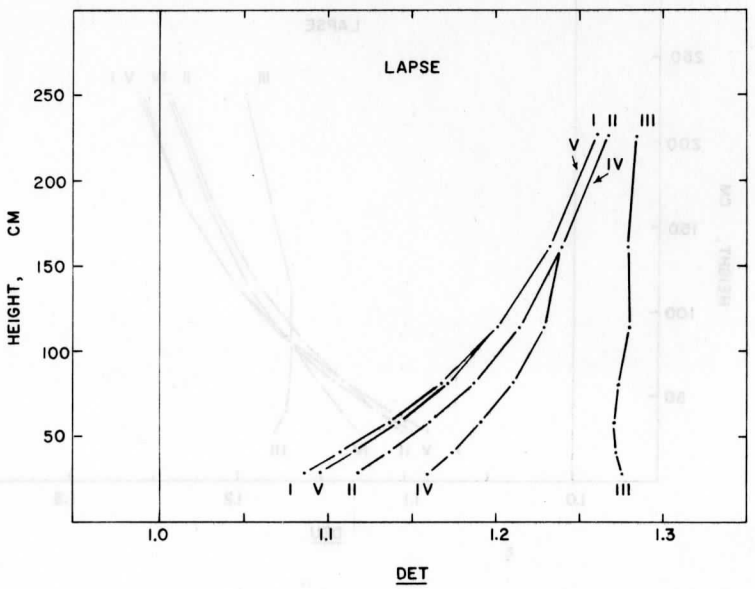

Fig. 4. Deacon number for potential temperature (DET) as a function of height for lapse temperature structure.

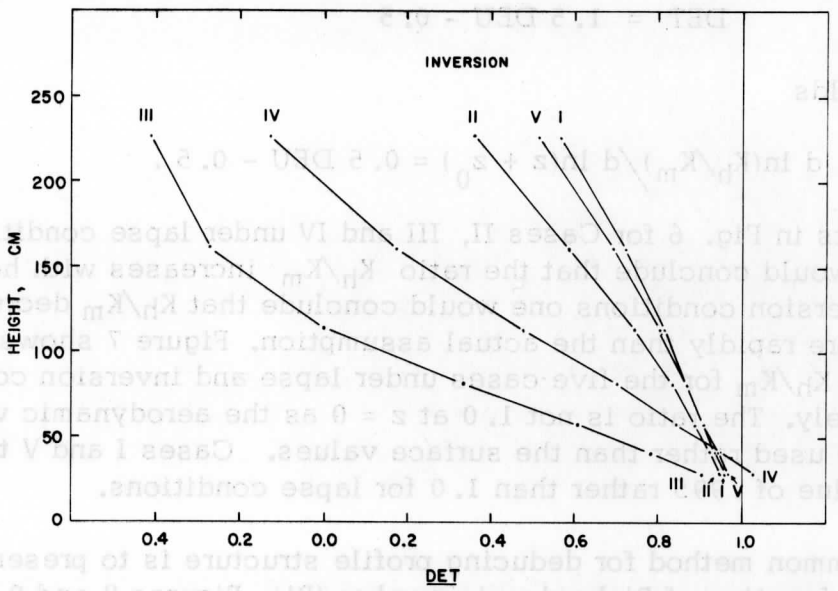

Fig. 5. Deacon number for potential temperature (DET) as a function of height for inversion temperature structure.

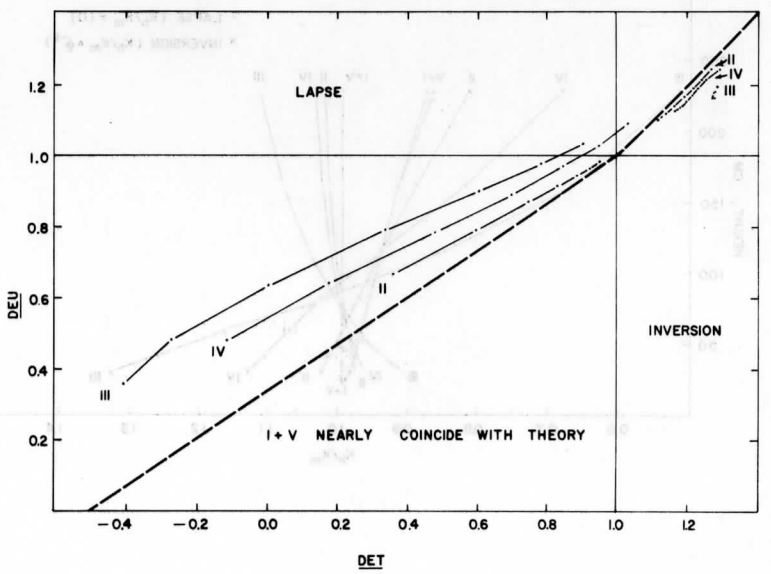

Fig. 6. DEU vs DET for inversion and lapse temperature structure. The dashed line is the theoretical curve used to construct the profiles of wind and temperature.

Under lapse conditions DET = DEU for $K_h/K_m = 1$ so (6) is zero. Under inversion conditions the assumption that $K_h/K_m = \phi^{-1/2}$ results in

$$DET = 1.5\ DEU - 0.5 \tag{7}$$

which yields

$$d\ \ln(K_h/K_m)/d\ \ln(z + z_0) = 0.5\ DEU - 0.5\ . \tag{8}$$

The results in Fig. 6 for Cases II, III and IV under lapse conditions show that one would conclude that the ratio K_h/K_m increases with height while under inversion conditions one would conclude that K_h/K_m decreases with height more rapidly than the actual assumption. Figure 7 shows the actual values of K_h/K_m for the five cases under lapse and inversion conditions, respectively. The ratio is not 1.0 at z = 0 as the aerodynamic values τ and Q are used rather than the surface values. Cases I and V thus have a K_h/K_m value of .995 rather than 1.0 for lapse conditions.

A common method for deducing profile structure is to present DEU and DET as a function of Richardson's number (Ri). Figures 8 and 9 present the results for lapse and inversion conditions. Cases I and V agree very

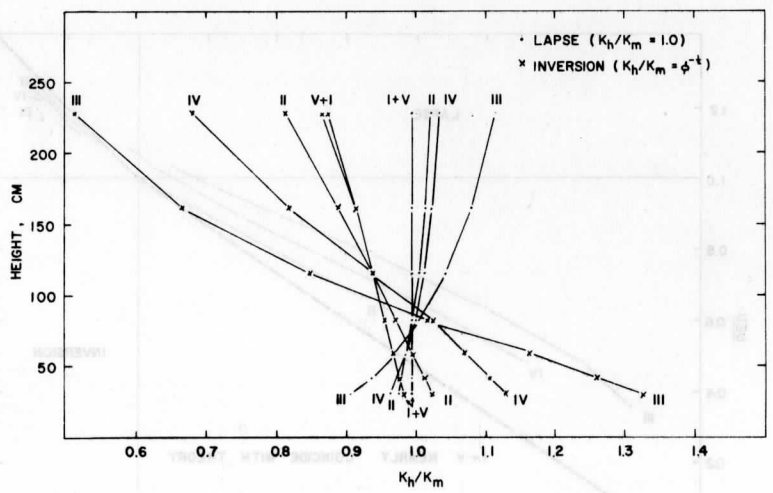

Fig. 7. The ratio K_h/K_m as a function of height. Case I for lapse and inversion temperature structure is the theoretical curve used for constructing the wind and temperature profiles.

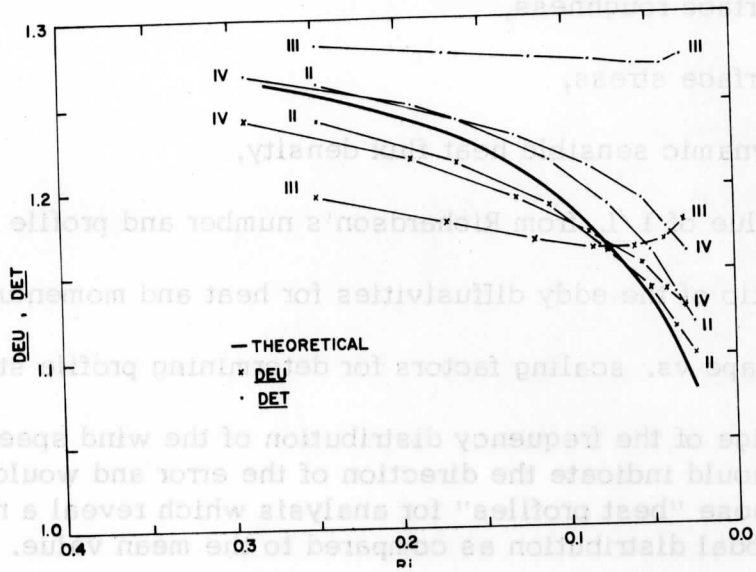

Fig. 8. DEU and DET as a function of Ri for lapse temperature structure. The heavy black line is the theoretical curve used to construct the wind and temperature profiles.

closely with the theoretical curve used to construct the profiles. Cases II, III and IV for lapse conditions indicate that the profile structures for wind and temperature are different. In Fig. 9 for inversion conditions one would conclude that for Cases II, III and IV the structure was quite different from the actual structure. Case IV represents the usually expected conditions (stress varying, heat flux constant) and possibly will be the most misleading.

4. Conclusions

Profile measurements of wind and temperature in the surface layer may be used for determining surface stress, sensible heat flux density and profile structure only if the wind speed and air temperature are linearly averaged over periods of time such that the surface stress and sensible heat flux density are nearly constant.

It is apparent that if wind speeds and air temperatures are averaged linearly over periods of time with varying fluxes, the following cannot be reliably determined:

a) the surface roughness,

b) the surface stress,

c) aerodynamic sensible heat flux density,

d) the value of 1/L from Richardson's number and profile theory,

e) the ratio of the eddy diffusivities for heat and momentum,

f) the shape vs. scaling factors for determining profile structure.

A knowledge of the frequency distribution of the wind speed and air temperature should indicate the direction of the error and would allow the selection of those "best profiles" for analysis which reveal a relatively narrow monomodal distribution as compared to the mean value.

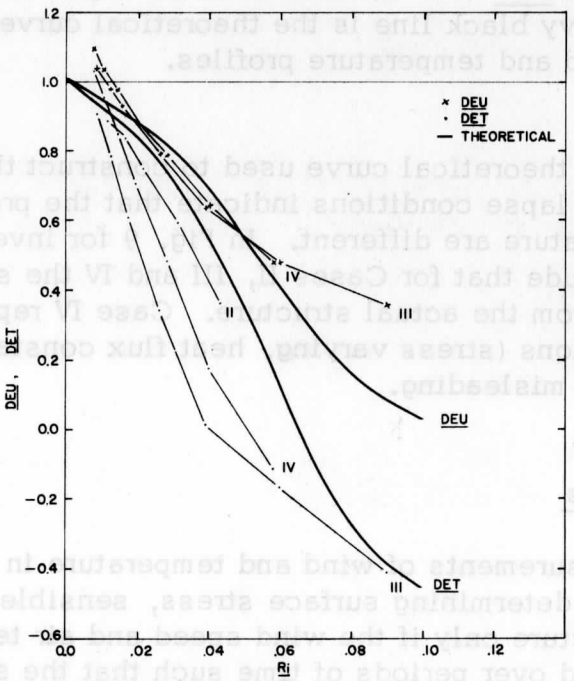

Fig. 9. DEU and DET as a function of Ri for inversion temperature structure. The heavy black line is the theoretical curve used to construct the wind and temperature profiles.

There are large quantities of profile data collected in the surface layer which have been analyzed to determine the above items. The discrepancies in the data are large and it is suggested that some of the discrepancies may be due to the common linear averaging process rather than a poor site or poor instrumentation. The problem is to determine when profile data was averaged over time periods with constant fluxes. Simple criterion such as a monomodal distribution of wind speed and air temperature must be used for determining when the fluxes or the wind speed and air temperature are sufficiently constant over the averaging time to provide fluxes within a desired tolerance.

5. References

Lettau, H. H.: 1962, Notes on Theoretical Models of Profile Structure in the Diabatic Surface Layer, Final Report, Contract DA-36-039-SC-80282 (USAEPG, Fort Huachuca, Arizona), University of Wisconsin, pp. 195-226.

Stearns, C. R.: 1967,"Micrometeorological studies in the coastal desert of Southern Peru," Ph. D. Thesis, Dept. of Meteorology, University of Wisconsin, 179 pp.

Stearns, C. R.: 1970a, Determining surface roughness and displacement height, Boundary Layer Meteorology, Vol. 1, No. 1, pp. 102-111.

Stearns, C. R.: 1970b, Conversion of profile difference quotients to true gradients at the geometric mean height, accepted for publication by Boundary Layer Meteorology.

Scanner's note:

This page is blank.

INTERCOMPARISON OF FLUX DENSITIES OF HEAT, MOISTURE AND MOMENTUM AT DAVIS, CALIFORNIA, 1967

Charles R. Stearns

1. Introduction

The Atmospheric Sciences Laboratory, U. S. Army Electronics Command, Fort Huachuca, Arizona sponsored a field experiment at the University of California, Davis from April 24 to May 6, 1967 known as the 1967 Cooperative Field Experiment. One of the purposes of the field experiment was to make intercomparison between several methods for measuring flux densities of sensible heat, latent heat and momentum. The results here presented are comparisons between profile estimates of the three above fluxes compared to a shear-stress lysimeter for stress, heat budget estimates of sensible and latent heat flux determined from a weighing lysimeter (Brooks and Pruit, 1966).

The profile data consisting of wind speed, air temperature and wet bulb temperature at nine levels to 320 cm at three points 100 m apart on an equilateral triangle are described by Stearns and Dabberdt (1967). A site description has been given by Brooks and Pruitt (1966).

2. Stress

Initially the aerodynamic stress (τ_0, dynes cm^{-2}) was determined by the method described by Stearns (1970) where the surface roughness (z_0, cm) and displacement height (d, cm) are determined so that the sum of the error squares on the friction velocity (V^*, cm) were a minimum. There were several occasions when z_0, d and τ_0 values were unrealistic when compared to the stress lysimeter and anemoclinometer (Tanner, 1970). Consequently, a value of $z_0 = 0.9$ cm and $d = 0.0$ for mast 1 and 2, and 2.0 cm for mast 3 were assumed to be reasonable and the stress recomputed. Figure 1 compares the average stress for the three masts to the stress as determined by the shear-stress lysimeter. All available data points were used for the indicated time period.

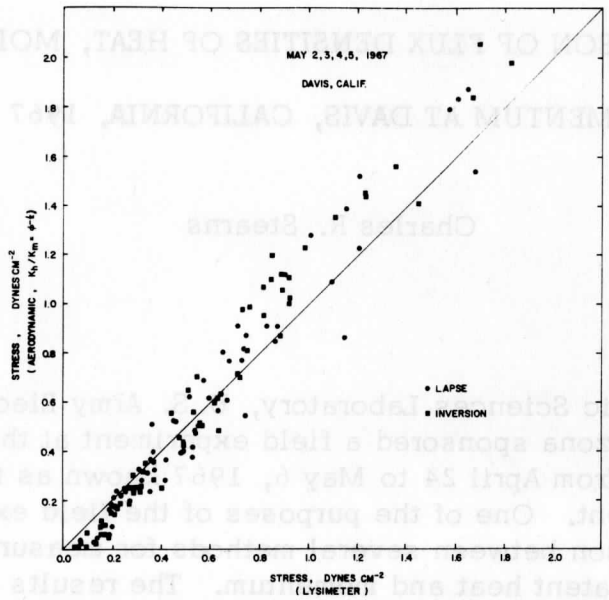

Fig. 1. Comparison between surface stress determined by the aerodynamic method assuming $K_h K_m^{-1} = \phi^{-1/2}$ and by the shear-stress lysimeter for 30 minute means collected at Davis, California. The light line at a 45 deg. angle indicates a 1:1 ratio.

It is to be expected that the shear-stress lysimeter is more likely to have a zero error than the profile method because of the difficulty in determining the zero position on the lysimeter as compared to determining zero wind speed. Figure 1 indicates the possibility of a zero error in the lysimeter amounting to less than 0.1 dynes cm^{-2}. The trend of the data in Fig. 1 indicates that the aerodynamic stress is about 0.2 dynes cm^{-2} higher than the lysimeter stress. The assumption that $K_h/K_m = 1$ or $\phi^{-1/2}$ (Stearns, Section 3) does not alter the stress value significantly but a lower value of z_0 and/or d would. Reducing the stress by changing z_0 and d would reflect lower values in the sensible and latent heat flux estimates by the aerodynamic method.

3. Sensible Heat Flux

An absolute measurement of the sensible heat flux density from surface to the air was not available compared to the shear-stress lysimeter for stress

and the weighing lysimeter for the latent heat flux density. The method readily available for comparison to the profile measurement of the sensible heat flux density is the heat budget approach.

The surface heat budget may be expressed as

$$R_n = S_0 + Q_0 + E_0 + P_0 \qquad (1)$$

where

R_n = net radiation

S_0 = soil heat flux density

Q_0 = sensible heat flux density

E_0 = latent heat flux density

P_0 = photo-chemical flux density

in units of ly min^{-1}. P_0 is neglected and assumed to be zero. The Bowen ratio $Q_0 E_0^{-1}$ is determined from 30 min mean potential temperature and specific humidity gradients, and the assumption that the eddy diffusivities for heat and moisture are equal. The set of equations used are as follows:

$$Q_0 = - \rho C_p K_h \theta' \qquad (2)$$

where

ρ = air density (gm cm^{-3})

c_p = specific heat of air (cal gm^{-1} k^{-1})

K_h = eddy diffusivity for heat cm^2 min^{-1}

θ = potential temperature gradient (k cm^{-1}),

and

$$E_0 = - \rho L K_e q' \qquad (3)$$

where

L = latent heat of vaporization (cal gm^{-1})

K_e = eddy diffusivity for moisture (cm^2 min^{-1})

q' = specific humidity gradient [(gm H_2O/gm air) cm^{-1}].

Then $Q_0 E_0^{-1} = + c_p K_h \theta' L^{-1} k_e^{-1} q'^{-1}$

$$= c_p L^{-1} K_h K_e^{-1} \theta' q'^{-1}, \quad (4)$$

and (1) becomes

$$Q_0 = \frac{R_0 - S_0}{1 + c_p^{-1} L K_h^{-1} K_e \theta' q'^{-1}} . \quad (5)$$

The assumption is made that $K_e K_h^{-1} = 1$. Then Q_0 at one mast is the sum of the Q_0's calculated for the temperature and moisture gradients calculated from 30 minute mean measurements at (20, 40), (40, 80), (80, 160) and (160, 320) cm levels. The three values at each of the three masts are averaged to obtain a final value for the 30 minute period which is assumed to be representative of the area enclosed by the three masts.

The three obvious deficiencies in the method are: 1. the difficulty inherent in measuring net radiation, 2. the assumption that $K_e K_h^{-1} = 1$, and 3. the assumption that the net radiation is the only source of heat.

The sensible heat flux density by the profile method is

$$Q_0 = - c_p \phi^{-1/2} \tau_0 \theta' V'^{-1} \quad (6)$$

where ϕ = the diabatic influence function (Lettau, 1962; Stearns, Sections 2 and 3),

V' = the vertical wind shear $\sec^{-1}$.

The assumption is made that $K_h K_m^{-1} = \phi^{-1/2}$ where $K_m = \tau_0 \rho^{-1} V'^{-1}$ is the eddy diffusivity for momentum. Q_0 is calculated utilizing eight values of V' and θ and τ_0^{-1} determined for the profile using the method in Section 2. The mean of the three profile masts is then assumed to be representative of the area enclosed by the three masts.

Figure 2 compares the sensible heat flux density obtained by the heat budget method to that obtained by the aerodynamic method. All points are included except those which overlap others especially under inversion conditions ($Q_0 < 0$). The usual scatter is present but under lapse conditions ($Q_0 > 0$) it appears that the aerodynamic method results in slightly higher values. This may be due to the high value of τ_0, the underestimation of net radiation or the horizontal advection of sensible heat into or out of the area enclosed by the three masts. There are differences between the three masts, but it is not yet known if the differences are significant.

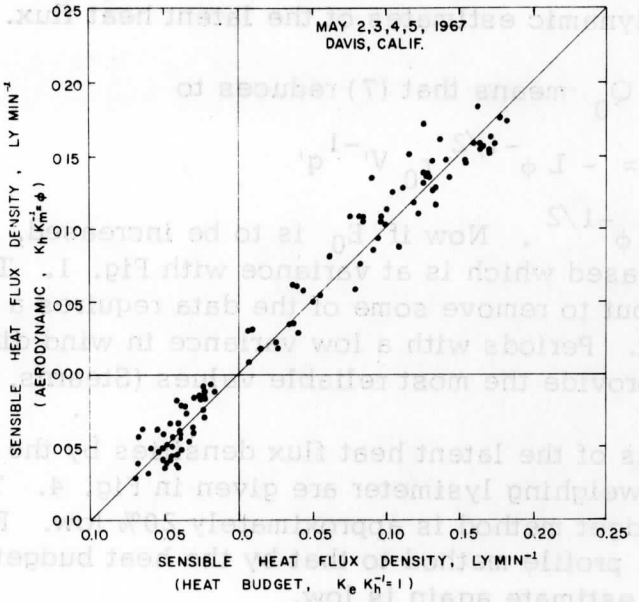

Fig. 2. Comparison between sensible heat flux densities determined by the aerodynamic and by the heat budget methods. The 45 deg. line indicates a 1:1 ratio.

4. Latent Heat Flux

The aerodynamic method for determining the latent heat flux (E_0, ly min^{-1}) is based on (3) and the assumption that $K_e K_h^{-1} = 1$. Then

$$E_0 = L c_p^{-1} Q_0 q' \theta'^{-1} \tag{7}$$

with q' and θ' determined from the same measurement points, Q_0 was previously determined for the particular mast system. The final value for each mast is the average using the several gradient measurements. The values for comparison to the weighing lysimeter, Fig. 3, are the three mast average with the exception of 30 min periods when the values at mast 3 are obviously in error due to partially dry wet bulbs. Figure 3 shows that the weighing lysimeter tends to yield slightly higher values of latent heat flux density. One could attribute this difference either to the horizontal advection of sensible heat into the area or possibly the ratio

$K_e K_h^{-1}$ is not equal to 1. The assumption that $K_e K_m^{-1} = 1$ results in still lower aerodynamic estimates of the latent heat flux.

The use of Q_0 means that (7) reduces to

$$E_0 = - L \phi^{-1/2} \tau_0 V'^{-1} q' \qquad (8)$$

where $K_e K_m^{-1} = \phi^{-1/2}$. Now if E_0 is to be increased, then τ_0 would have to be increased which is at variance with Fig. 1. The scatter of Fig. 3 is large but to remove some of the data requires a reason which is not yet apparent. Periods with a low variance in wind direction or air temperature might provide the most reliable values (Stearns, Section 3).

Comparisons of the latent heat flux densities by the heat budget method to those by the weighing lysimeter are given in Fig. 4. The indication is that the heat budget method is approximately 20% low. Figure 5 compares $E_0 + Q_0$ for the profile method to that by the heat budget indicating that the heat budget estimate again is low.

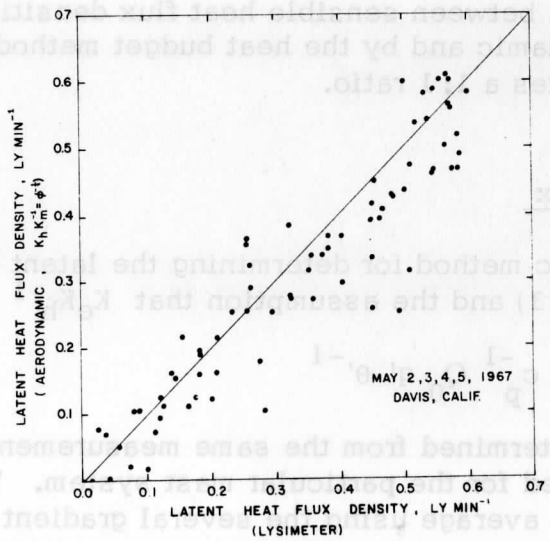

Fig. 3. Latent heat flux density by the aerodynamic method compared to the weighing lysimeter. The 45 deg. line indicates a 1:1 ratio. Negative values were near zero and not included.

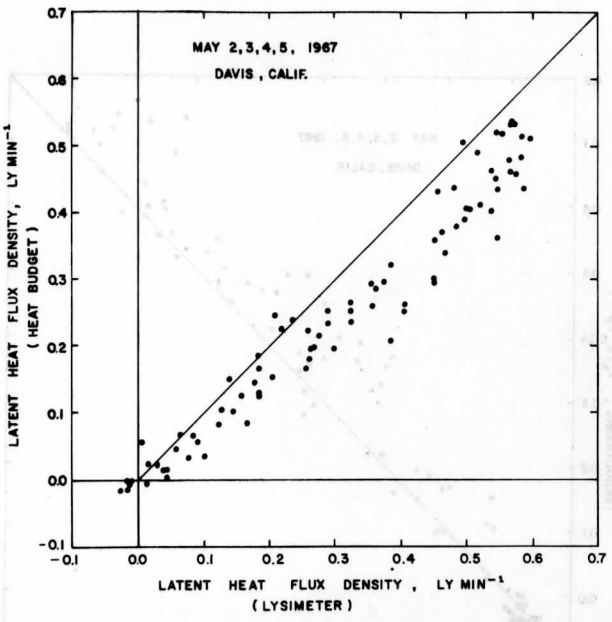

Fig. 4. Latent heat flux density by the heat budget method compared to the weighing lysimeter. The 45 deg. line indicates a 1:1 ratio.

5. Conclusions

The scatter in the data indicates the difficulty in drawing conclusions about ratios such as $K_h K_m^{-1}$, $K_e K_m^{-1}$ and $K_e K_h^{-1}$. The assumption that $K_e K_m^{-1} = K_h K_m^{-1} = \phi^{-1/2}$ gives solutions for all times under lapse and inversion conditions which compare within approximately 20% to the shear-stress and weighing lysimeters. The profiles have not been selected in any way but such a procedure as using only periods with small deviations in a parameter such as wind speed, wind direction or air temperature might eliminate some of the scatter in the data. Lettau (Section 1) points out some of the requirements necessary to use diffusivities and Stearns (Section 3) shows how linear time averaging of wind speed and air temperature can drastically alter the diffusivity ratios yielding misleading results which are in the directions accepted by many investigators (Lumley and Panofsky, 1964).

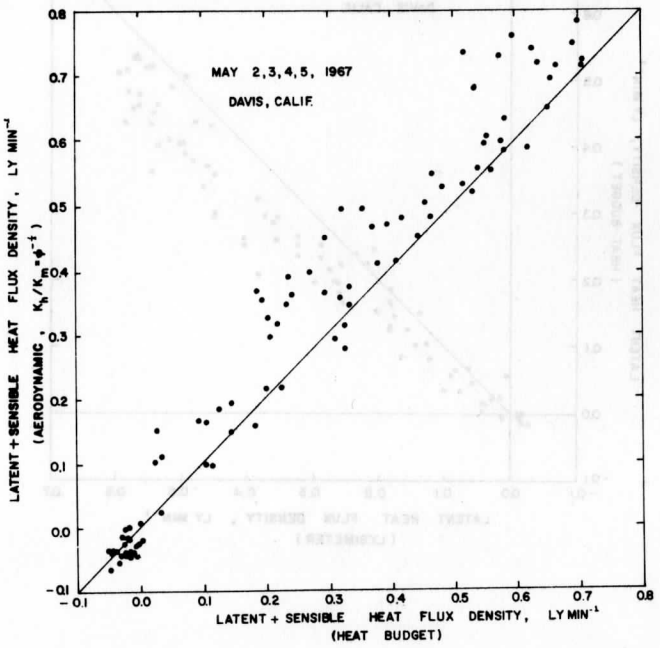

Fig. 5. The sum of latent and sensible heat flux densities by the aerodynamic and the heat budget methods show that the heat budget method indicates a lower value than the aerodynamic method. The 45 deg. line indicates a 1:1 ratio.

6. References

Brooks, F. A., and W. O. Pruit, 1966: Investigation of Energy, Momentum and Mass Transfers Near the Ground, Final Report, Grant DA-AMC-28-043-65-G12 (USAEC, Fort Huachuca, Arizona), University of California, Davis, California.

Stearns, C. R., 1970: Determining surface roughness and displacement height, Boundary-Layer Meteorology, Vol. 1, pp. 102-111.

Stearns, C. R., and W. F. Dabberdt, 1968: Collections and Processing of Micrometeorological Data for the Spring, 1967, Cooperative Field Experiment at Davis, California, Final Report, Contract No. DAADO-67-C-0117 (USAEC, Fort Huachuca, Arizona), University of Wisconsin, Madison, Wisconsin.

Lumley, J. L., and H. A. Panofsky, 1964: The Structure of Atmospheric Turbulence, John Wiley and Sons, New York.

DIURNAL THERMO-TIDAL WINDS OVER SLOPING TERRAIN*

Kenneth P. MacKay, Jr.

ABSTRACT: This study presents an extension of Lettau's (1964, 1967) theory of thermo-tidal winds, defined as winds in the boundary layer caused by diurnal solar forcing and of large enough horizontal extent so that Coriolis effects are important. Specifically considered is the case of diurnal solar heating in the atmospheric boundary layer over continental areas with a large scale terrain slope.

The first harmonic of the geostrophic wind oscillation is derived from an expression for the vertical propagation of the diurnal temperature wave in the boundary layer over sloping terrain. While this geostrophic forcing function has an afternoon maximum over the Great Plains, investigation of the response shows that the wind has a nighttime maximum. Analysis of available data shows that those observation periods for which the observed temperature distribution conformed with model criteria showed fairly good agreement between observed and predicted wind oscillation characteristics. Conversely, those periods during which the observed temperature distribution did not conform with model criteria were not characterized by wind distributions which approximated those predicted by the model.

An attempt has been made to combine the effects of diurnal oscillations in geostrophic wind and internal friction by using in the equations of motion an height-independent eddy diffusivity for momentum which has a sinusoidal oscillation in time. It is found that the mean wind and the first and second harmonic oscillations are mutually coupled. The 24-hour hodograph corresponds to a slightly modified Ekman spiral if reasonable values of the amplitude of the eddy diffusivity oscillation are used. The first harmonic wind

*Portions of this paper have been extracted from a Ph. D. thesis by Kenneth P. MacKay, Jr., entitled "Thermal Tidal Winds over Sloping Terrain" (1970), submitted to the Department of Meteorology, University of Wisconsin.

oscillation is, in general, greater than the response to an oscillating geostrophic wind alone, but the theoretical wind response has a complicated relationship with latitude and eddy diffusivity oscillation amplitude. Data indicate that theoretical second harmonic wind amplitude and phase profiles approximate those observed, but the theoretical model in its present form is insufficient to explain these features.

1. Introduction

Evidence of diurnal wind oscillations in the planetary boundary layer has been reported in Africa (e. g. Goualt, 1938), South America (Lettau, 1967), and North America (e. g. Blackadar, 1957 and Bonner, 1968).

Over the United States these oscillations are most pronounced over the Great Plains in summer (Bonner, 1968). The southerly nocturnal wind maximum at about 500 meters above the ground surface seems to be associated with summer nocturnal thunderstorms in the area (e. g. Bleeker and André, 1951, and Pitchford and London, 1962).

Darkow and Thompson (1967) have suggested that the boundary layer wind oscillations over the United States may propagate upward and excite the oscillations in the free atmosphere found by Hering and Borden (1962).

The influence on boundary layer wind oscillations of the large scale terrain slope from the Rocky Mountains to the Mississippi River has been recognized by Lettau (1964, 1967), Holton (1967), and Paegle (1969), among others.

The equation of motion describing accelerations of the horizontal wind is written in complex vector notation as

$$\frac{dV}{dt} = -\rho^{-1}\nabla_H P - ifV - \alpha\tau_z , \qquad (1.1)$$

where $V = u + iv$ is the complex horizontal wind vector, ρ the density for dry air (assumed constant), P pressure; $f = 2\omega \sin\phi$ is the Coriolis parameter, ω the angular velocity of the earth, ϕ latitude, $\tau = \tau_1 + i\tau_2$ the shearing stress vector, $i = (-1)^{1/2}$, x and u are positive along the real axis, y and v along the imaginary axis. The subscripts 1 and 2 are used where necessary to avoid confusion to denote vector components along the real and imaginary axes, respectively. The two-dimensional operators are: $d(\ )/dt = (\ )_t + u(\ )_x + v(\ )_y$, the derivative following the mean motion; $\nabla_H = (\ )_x + i(\ )_y$, the horizontal gradient operator; subscripts denote partial differentiation with respect to the subscripted independent variable.

The first term on the right side of (1.1) expresses the influence of horizontal pressure gradients. It is convenient to express the pressure gradient force in terms of the geostrophic wind vector $G = U_1 + iU_2$, viz.

$$-\rho^{-1}\nabla_H P = ifG \tag{1.2}$$

The vertical shear of the geostrophic wind, G_z, is known as the thermal wind. Combining (1.2) with the equation of state of an ideal gas and the hydrostatic equation, the thermal wind can be expressed as

$$G_z = i\frac{g}{fT}\nabla_H T + \frac{T_z}{T}G, \tag{1.3}$$

where T is the absolute temperature.

The first term on the right of (1.3) is the contribution of horizontal temperature gradients to the vertical shear of the geostrophic wind. This term indicates that in the northern hemisphere the thermal wind vector is parallel to the isotherms on a horizontal surface with low temperature to the left. The second term is a correction involving the vertical temperature gradient and the slope of isobaric surfaces. This term is small enough so that it is often neglected (Haltiner and Martin, 1957). However, when it is neglected in later derivations, I will so state.

The second term on the right of (1.1), notwithstanding some doubt concerning historic claims to priority (see e.g. Jordan, 1966), is known as the Coriolis force and expresses the influence of the earth's rotation. This effect acts to turn winds to the right in the northern hemisphere.

Atmospheric motions are fully turbulent except in a shallow (of the order of a centimeter deep) sublayer at the earth's surface. Turbulent eddy stresses are much larger than molecular stresses, thus the last term of (1.1), which is the frictional force, is given in terms of the vertical variation of the eddy stress. Similarities between laminar and turbulent flow suggest the definition of an effective eddy diffusivity for momentum, K, such that

$$\tau = \rho K V_z \tag{1.4a}$$

If the assumption is made that K and ρ are independent of height, the vertical variation of τ is

$$\tau_z = \rho K V_{zz}. \tag{1.4b}$$

Properties of the shearing stress vector can be used to single out the lowest stratum of the layer of frictional influence. This stratum, after the

definition introduced by Lettau (see Lettau and Davidson, 1957, chapter 7), is named the surface layer and is defined as that layer through which $|\tau|$ departs by only a few percent from its surface value. The depth of the surface layer is of the order of 10 to 100 m (Sutton, 1953).

Lettau (1967) has discussed wind dynamics in the boundary layer in terms of forcing function and response, analogous to a passive electrical circuit responding to an applied voltage or a seismograph responding to an earth tremor. He shows the utility of viewing wind motion as a response to the applied forcing of the pressure pattern, expressed as variations of the geostrophic wind. In this light (1.1) is written, after substitution of (1.4b) and (1.2) and neglecting the inertia terms of dV/dt, as

$$V_t - KV_{zz} + ifV = ifG . \qquad (1.5)$$

Atmospheric motions described by (1.5) can be classified in terms of the magnitude of the forces and accelerations involved. Jeffries (1929), for example, introduced the term "antitriptic" to describe flow dominated by the friction and pressure gradient forces. Johnson (1966) suggested that winds resulting from a balance between the pressure gradient force, the Coriolis force and the internal friction force be called "geotriptic."

More recently, Lettau (1964, 1967), has termed "thermo-tidal" those winds in the boundary layer caused by solar forcing and of large enough lateral extent so that the Coriolis force is significant. Analogous to the Glossary of Meteorology definition of a thermal tide as "a variation in atmospheric pressure due to the diurnal differential heating of the atmosphere by the sun...," thermo-tidal theory reasons that the diurnal heating cycle can, under certain circumstances, produce a variation in atmospheric pressure gradient.

The sea breeze is confined to the boundary layer, is caused by solar forcing and may, if very well developed, have a large enough lateral extent for the Coriolis force to be significant. However, more often than not, the latter condition will not be met (Jeffries, 1929). In any case, the sea breeze will be excluded from the definition of thermo-tidal winds.

Over a large scale terrain slope, we can reason as follows: The diurnal cycle of insolation produces a diurnal oscillation of sensible heat transfer between earth surface and atmosphere. The heat transfer, being normal to the earth's surface, produces an oscillation in the temperature gradient measured in a direction mutually perpendicular to the ground surface and the terrain fall line. The oscillation of the temperature gradient normal to the sloping terrain causes an oscillation in the horizontal temperature gradient measured along a surface at a constant height above sea level. The variation in horizontal temperature gradient will

produce oscillations in the thermal wind, leading to diurnal oscillations in the geostrophic wind. The oscillating geostrophic forcing function in (1.5) causes an oscillation in the wind vector.

The purpose of this investigation is to attempt an extension of the mathematical description of the dynamics of the thermo-tidal wind and to compare the model with available data.

2. Terrain Influence on Diurnal Wind Oscillations

Two models of the development of LLJ oscillations have generated interest in recent years: the theory based on diurnal oscillation of frictional forces as proposed by Blackadar (1957) and models based on thermal wind oscillation due to the diurnal heating cycle over a large scale topographical slope as suggested by Lettau (1964, 1967), and by Holton (1967).

Blackadar (1957) reasoned that soon after a surface nocturnal inversion is established, turbulent mixing dies out above the inversion. The friction force acting on the wind decreases, which disturbs its balance with the pressure gradient and Coriolis forces, producing an acceleration in the geostrophic departure above the inversion, which can be constant in magnitude but rotating with the inertial period. This essentially free inertial oscillation reaches a supergeostrophic maximum about six pendulum hours after sunset. Below the top of the inversion, momentum is being transported to and dissipated by the ground, and the wind profile should have its maximum at the inversion level. Blackadar suggests that within the nocturnal inversion layer the loss of momentum should be proportional to the loss of heat, and therefore the wind and temperature profiles should resemble each other.

Buajitti and Blackadar (1957) and Haltiner (1959) attempted numerical solutions of the appropriate forms of the equations of motion with numerous forms of eddy viscosity varying with height and time. While several main features of the diurnal variation in the wind profile were reproduced, none of the computed solutions adequately explained the observed diurnal wind structure variations.

Blackadar's model fails to explain the observed concentration of nocturnal low-level wind maxima in a relatively narrow band from Texas to Nebraska. If the diurnal variation of internal friction were the only cause of the diurnal wind oscillation and the characteristic nocturnal low-level jet profile, then one would expect to find these wind phenomena over other parts of the continent if there is a strong diurnal heating cycle.

Blackadar has shown that the height of maximum wind in 88 jet profiles at Drexel, Nebraska, coincided well with the top of the surface inversion. Bonner (1965) found that the correlation coefficient between level of maximum wind and inversion height was 0.53 for 52 observations near the core of his 28 day average jet stream. In the majority of cases, the base of the inversion was several hundreds of meters above the ground. Hoecker (1963) found one jet (22-23 April, 1961) which persisted during the day in lapse condition below an inversion aloft.

Due to the decrease of the period of inertial oscillation by about 50 percent between southern Texas and northern Minnesota, Blackadar's model predicts a corresponding change in the rate of turning of the geostrophic departure vector, while in fact the turning rate is about 15 deg hr^{-1} at both locations (Bonner, 1965). Average rates of turning of 13.5 deg hr^{-1} at 600 m and 17 deg hr^{-1} at 1000 m derived by Blackadar (1957) from observations at O'Neill would seem closer to the diurnal frequency of 15 deg hr^{-1} than his predicted 20.2 deg hr^{-1} .

Recently Paegle (1969) has extended Ooyama's (1957) solutions incorporating a form of K constant with height and varying sinusoidally in time. He concludes that this form of K cannot explain the large amplitudes in wind oscillations sometimes observed.

Lettau (1967), in an extension of an earlier (1964) note, presented a simplified model for the influence of topography on the temperature structure in the planetary boundary layer and the resulting effect on the dynamics of the wind. He emphasized the need to consider an existing coupling between topographical gradient and average or prevailing horizontal pressure gradient; for instance, an average pressure gradient positive to the east as elevation increases to the west, corresponds to the common situation of southerly flow over the Great Plains as a result of the Bermuda High and a Rocky Mountain low. In this example, Lettau's reasoning leads to the conclusion that the steady state thermal wind should be from the north.

In describing the effects of the diurnal heating cycle on the geostrophic wind profile, Lettau assumed no temperature gradient along the ground surface and that isotherms in the atmosphere remain parallel to the earth's surface during the day, producing an oscillating horizontal temperature gradient in the air above a terrain slope. The oscillating temperature gradient would in turn produce diurnal oscillations in the geostrophic and thermal winds. For the area of the Great Plains, the southerly geostrophic wind speed would decrease with height in lapse conditions during the day and increase with height to the top of the inversion layer at night. In his numerical example, the geostrophic wind would increase from 10 m

sec^{-1} at the surface to 15 m sec^{-1} at 400 m, if the temperature inversion were 6C over the same depth.

Lettau applied the term thermo-tidal winds to oscillations of horizontal winds caused by heating cycles of diurnal frequency, provided that the horizontal scale of the circulation is of sufficient extent so that Coriolis effects are significant. The geostrophic wind oscillation produced by the diurnal heating cycle can be viewed as a forcing function. The properties of the diurnal oscillation of the wind are then responses to this geostrophic forcing function.

The phase angles of the geostrophic forcing function assumed by Lettau and later by MacKay (1969), however, disagree with the time variation of the surface geostrophic wind observed by Hoecker (1965) and Sangster (1967). The form of G used by Lettau (1967) assumed that the maximum surface geostrophic wind occurs near local midnight and that the time of maximum was constant with height. MacKay presented solutions of (1.5) for a number of assumed forms of G all of which had a surface maximum at or near local midnight.

Hoecker (1965) presented graphs of sea level geostrophic wind values indicating maximum values at about noon (1200) CST for his three jet development days.

Later, Sangster (1967, 1968) computed southerly surface geostrophic winds along the sloping terrain utilizing a pressure gradient equation derived from Bellamy's (1945) altimeter correction system. He established the diurnal cycle in the surface geostrophic wind component parallel to the smoother terrain contours averaged over 30 days of June 1966 for each hour of the day. The cycle maximum occurred at 1600 CST, the minimum at 0600 CST, with a range of about 18 knots. For two individual case studies in the same region he found similar oscillations with maxima occurring at about 1700 CST, minima about 0500 CST and night to day ranges of 18 to 24 knots.

The results of Hoecker and Sangster indicate that the surface geostrophic wind in the Oklahoma area at least for days with generally southerly flow has a daily cycle with a maximum in the afternoon.

Paegle (1969) states that the resonance phenomena exhibited by Lettau's (1964) solution at 30° latitude where the amplitude of the wind response becomes infinite and the phase angle changes sign do not agree with initial value solutions for a geostrophic oscillation in the boundary layer.

He presents a periodic solution similar to that presented by MacKay (1969) for an oscillation in G whose amplitude attenuates exponentially in the vertical. The properties of the wind oscillations predicted by MacKay and Paegle are similar. Paegle notes that the solution does not blowup at 30° latitude and that there is no sign change in the phase angle but a continuous change as one passes from latitudes 45° to 23°.

Neither Paegle nor MacKay have specifically noted that the 30° resonance phenomenon predicted by Lettau's model is due solely to the assumption of a linear decrease in the amplitude of the oscillating part of G. However, this result can be seen by comparing the solutions presented by MacKay for linear and exponentially decreasing amplitudes in the G oscillation.

Holton (1967) has shown that the thermodynamic energy equation and the equations of motion are coupled when expressed in a slope coordinate system, and that the diurnal heating cycle can be the forcing function for the diurnal wind oscillation. Holton's model is strictly valid only at 30° latitude but may be extended to other latitudes.

Holton predicted that the v-component of the wind in a geostrophic system should show the maximum about six hours after the time of maximum surface temperature. Phase angles derived from data at O'Neill (Lettau, 1967) indicate that the v-component has its maximum at about local midnight near the surface, much later than six hours after the time of surface temperature maximum. Paegle (1969) also notes the discrepancy in predicted and observed phase hour.

In summary, it can be said that phase angles of the geostrophic forcing function assumed by Lettau (1964, 1967) and by MacKay (1969) do not agree in certain respects with observations by Hoecker (1965) and Sangster (1967). The theoretical wind response predicted by Holton (1967) also disagrees with the properties of the wind oscillation determined from observations. Therefore, an attempt will be made to derive a new form of the geostrophic forcing function and to determine the resulting wind response.

In order to derive the influence of the diurnal temperature oscillation on the geostrophic forcing function, assume a surface temperature oscillation of the form

$$T_0 = \bar{T}_0 + T_0' \cos \omega t \,,$$

where T_0 is the surface temperature, T'_0 is the amplitude of the surface oscillation about the mean and $t = 0$ at the time of maximum temperature.

Assuming an eddy diffusivity for heat, κ, which is constant with height and time, the equation governing heat propagation through the boundary layer is

$$T_t = \kappa T_{zz} .$$

The classical solution for the first harmonic of the temperature wave, T', is (see Sutton, 1953),

$$T' = T'_0 e^{-\sqrt{\omega/2\kappa}\, z} \cos(\omega t - \sqrt{\omega/2\kappa}\, z).$$

Introducing for later convenience the parameter ε where $\varepsilon = (\omega K/f\kappa)^{1/2}$

$$T' = T'_0 e^{-\varepsilon \eta z} \cos(\varepsilon t - \varepsilon \eta z). \qquad (2.1)$$

The geostrophic wind G has the assumed form

$$G = \bar{G}(z) + G'(z, t)$$

where the 24-hour mean geostrophic wind profile, $\bar{G}$, is given by $\bar{G} = \bar{G}_0 + (\bar{G}_* - \bar{G}_0)(1 - e^{-a\eta z})$ where $\bar{G}_0$ = mean surface geostrophic wind, $\bar{G}$ = the mean geostrophic wind at the top of the boundary layer, $(\bar{G}_* - G_0) = \bar{V}G$ is the geostrophic shear vector; where $\eta' = \sqrt{2}\eta$ is introduced to scale the height parameter and $a = b/\eta'$ where b is an empirical constant representing the rate of change of curvature of the temperature profile with height and $\eta = (f/2k)^{1/2}$ where f = Coriolis acceleration and k is the eddy diffusivity for momentum. $G' = U'_1 + iU'_2$ represents the amplitude of the diurnal oscillating component; the imaginary axis is parallel to the smoothed terrain contours.

The oscillating thermal wind $G'_z = U'_{iz} + iU'_{zz}$ is, if θ is small, given by the approximations

$$U'_1 = U_{1z} = 0$$

$$U'_{2z} = -\frac{g\theta}{f\bar{T}_0} T'_z .$$

Integrating over z,

$$G' = C - \frac{g\theta}{f\bar{T}_0} T' ,$$

where C is a constant of integration. Assuming that the amplitude of the oscillating G' dies out at great heights, $C = 0$ and

$$U'_2 = -\frac{g\theta}{f}\frac{T'_0}{\bar{T}_0} e^{-\varepsilon\eta z}\cos(\omega t - \varepsilon\eta z). \tag{2.2}$$

In the Great Plains area, θ will be negative and (2.2) states that the oscillations of the surface geostrophic wind and surface temperature will be in phase. Sangster's analysis seems to indicate that the geostrophic wind lags the temperature cycle by four to five hours. Although there is some uncertainty about the time of maximum of the surface geostrophic wind, we shall take the time origin in (2.2) to be the time of this maximum.

Letting $g = 10$ m sec^{-2}, $\theta = -2 \times 10^{-3}$, $f = 10^{-4}$ sec^{-1}, $(T'_0/\bar{T}'_0 = 10/300)$, the surface geostrophic oscillation will have an amplitude of 7 m sec^{-1}, or a daily range of approximately 27 knots, in rough agreement with Sangster's estimates.

We now express G' as

$$G'(z, t) = G_1(z)e^{i\omega t} + G_2(z)e^{-i\omega t}. \tag{2.3}$$

Equation (2.2) can be written as

$$U'_2 = U_g e^{-\varepsilon\eta z}[e^{i(\omega t - \varepsilon\eta z)} + e^{-i(\omega t - \varepsilon\eta z)}] \tag{2.4}$$

where

$$U_g = -\frac{g\theta}{2f}\frac{T'_0}{\bar{T}_0},$$

comparing (2.3) and (2.4),

$$G_1 = i\,U_g e^{-(1+i)\varepsilon\eta z}$$

$$G_2 = i\,U_g e^{-(1-i)\varepsilon\eta z} \tag{2.5}$$

The complex wind response is defined to be

$$V(z, t) = \bar{V}(z) + V_1(z)e^{i\omega t} + V_2(z)e^{-i\omega t} \tag{2.6}$$

Substituting (2.4), (2.5) and (2.6) into (1.5) and separating identical powers of $e^{\varepsilon\eta\omega t}$, $-1 \le \eta \le 1$, results in three ordinary differential equations for $\bar{V}$, V_1 and V_2:

$$\bar{V}_{zz} - 2i\eta^2 \bar{V} = -2i\eta^2 \bar{G} \tag{2.7a}$$

$$V_{1zz} - 2i\eta^2 \alpha V_1 = 2\eta^2 V_g e^{-(1+i)\varepsilon\eta z} \tag{2.7b}$$

$$V_{2zz} \pm 2i\eta^2 \beta^2 V_2 = 2\eta^2 U_g e^{-(1-i)\varepsilon\eta z} \tag{2.7c}$$

The appropriate boundary conditions are $\bar{V}(z=0) = V_1(0) = V_2(0) = 0$, $\bar{V}(\infty) = \bar{G}(\infty)$ and $V_1(\infty) - V_2(\infty) = 0$. The parameters introduced are $\alpha^2 = 1 + \omega/f$, $\beta^2 = |1 - \omega/f|$; the upper sign in (2.7c) applies to latitudes poleward of 30° while the lower sign applies equatorward.

The solutions are

$$V_1/V_g = i(e^{-(1+i)\alpha\eta z} - e^{-(1+i)\varepsilon\eta z})/(\varepsilon^2 - \alpha^2)$$

$$V_2/V_g = i(e^{-(1-i)\varepsilon\eta z} - e^{-(1\pm i)\beta\eta z})/(\varepsilon^2 + \beta^2)\,. \tag{2.8}$$

If the real velocities are to be written as

$$u(z,t) = \bar{u}(z) + u_1(z)\cos\omega t + u_2(z)\sin\omega t$$

$$v(z,t) = \bar{v}(z) + v_1(z)\cos\omega t + v_2(z)\sin\omega t\,, \tag{2.9a}$$

it follows that

$$\bar{u} = RE(\bar{V}) \qquad \bar{v} = IM(\bar{V})$$

$$u_1 = RE(V_1 + V_2) \qquad v_1 = IM(V_1 + V_2)$$

$$u_2 = IM(V_2 - V_1) \qquad v_2 = RE(V_1 - V_2)\,, \tag{2.9b}$$

where

$$\left.\begin{aligned} u_1 &= \frac{e^{-\alpha\eta z}\sin\alpha\eta z}{\varepsilon^2 - \alpha^2} \pm \frac{e^{-\beta\eta z}\sin\beta\eta z}{\varepsilon^2 + \beta^2} - e^{-\varepsilon\eta z}\sin\varepsilon\eta z\left[\frac{1}{\varepsilon^2 - \alpha^2} + \frac{1}{\varepsilon^2 \pm \beta^2}\right] \\ u_2 &= \frac{e^{-\alpha\eta z}\cos\alpha\eta z}{\varepsilon^2 - \alpha^2} - \frac{e^{-\beta\eta z}\cos\beta\eta z}{\varepsilon^2 \pm \beta^2} + e^{-\varepsilon\eta z}\cos\varepsilon\eta z\left[\frac{1}{\varepsilon^2 - \alpha^2} + \frac{1}{\varepsilon^2 \pm \beta^2}\right] \end{aligned}\right\}$$

$$v_1 = \frac{e^{-\alpha\eta z}\cos\alpha\eta z}{\varepsilon^2 - \alpha^2} - \frac{e^{-\beta\eta z}\cos\beta\eta z}{\varepsilon^2 + \beta^2} - e^{-\varepsilon\eta z}\cos\varepsilon\eta z\left[\frac{1}{\varepsilon^2 - \alpha^2} - \frac{1}{\varepsilon^2 \pm \beta^2}\right]$$

$$v_2 = \frac{e^{-\alpha\eta z}\sin\alpha\eta z}{\varepsilon^2 - \alpha^2} \pm \frac{e^{-\beta\eta z}\sin\beta\eta z}{\varepsilon^2 \pm \beta^2} - e^{-\varepsilon\eta z}\sin\varepsilon\eta z\left[\frac{1}{\varepsilon^2 - \alpha^2} - \frac{1}{\varepsilon^2 \pm \beta^2}\right] \Bigg\} \qquad (2.10)$$

The amplitude of the u and v oscillations will be given as

$$\text{u amp} = (u_1^2 + u_2^2)^{1/2}$$

$$\text{v amp} = (v_1^2 + v_2^2)^{1/2} \qquad (4.11a)$$

and the phase constants as

$$\text{u-phase} = \frac{\pi}{12}\,\text{arc tan}(u_2/u_1)$$

$$\text{v-phase} = \frac{\pi}{12}\,\text{arc tan}(v_2/v_1)\,, \qquad (2.11b)$$

where u-phase and v-phase are the times of maximum of the respective oscillations given as hours after the time of maximum surface geostrophic wind.

The wind response function, normalized to the amplitude of the surface geostrophic wind oscillation is completely defined by amplitudes and phase angles (2.11). These, in turn, are functions only of height, latitude and the ratio of the eddy diffusivities for momentum and heat, K/κ.

Consider the wind response equatorward of 30° latitude as expressed by (2.8). The ratio ω/f will be large at low latitudes and will decrease rapidly proceeding poleward. Therefore, the exponential terms in (2.8) involving α and β will be small and the denominators of each term will be large. This means that the wind response amplitude will be negligible near the equator and will increase rapidly as latitude increases toward 30°.

At 30° latitude, β vanishes, and the expression for V_2 becomes

$$\frac{V_2}{U_g} = -i\frac{\kappa}{K}\left[1 - e^{-(1-i)\varepsilon\eta z}\right] \qquad (2.12)$$

which is similar to the Ekman spiral solution. V_2 does not vanish at great heights, which indicates that the assumptions made in the formulation of the problem do not hold near 30°.

At 30° latitude, the diurnal wind cycle is driven at the frequency resonant with the natural mode of oscillation of the rotating atmosphere. As Paegle (1969) notes, this resonance would lead to infinite winds in the absence of viscosity. However, turbulent momentum diffusion to the ground and to higher levels is rapid enough to avert infinite winds if the forcing is confined to a finite layer. He also notes that forcing at low levels, even though negligible aloft, causes the response amplitude to be finite at all levels. He concludes that geostrophic balance cannot be a reasonable upper boundary condition at 30°.

At large heights, V_1 will approach zero and substitution of (2.12) into (2.9b) shows that $v_1 = u_2 = -\kappa/K$ and $v_2 = u_1 = 0$. Thus, at 30° latitude, both the u- and v-amplitudes will approach κ/K. Relative to the geostrophic wind oscillation, the u- component will lag by 18 hours, the v-component by 12.

The wind responses poleward of 30° are not as readily discernable from an inspection of the solutions. Therefore, graphical presentations are given in Figs. 2.1 and 2.2 to delineate the influence of the relevant parameters.

Figure 2.1 illustrates the previous discussion, showing a rapid increase in amplitude with increasing latitude to a maximum at 30° which is about 10% greater than the ratio κ/K. Poleward of 30° there is a rapid decrease in amplitude to about 35° and then the amplitude is relatively constant as latitude increases. Equatorward of 30° the down-slope wind amplitude is greater than the cross-slope, poleward of 30° the reverse is true.

The phase relationships show only minor variations on each side of 30°. Equatorward the down-slope (u) component lags the surface geostrophic wind by about 18 hours, the cross-slope (v) by 12 to 13 hours. Between 30 and 35° latitude there is a phase shift of three to six hours so that poleward of 35° the u component lags by about 13 hours, the v-component about six.

Figure 2.2 depicts the height profiles of the response amplitude and phase hours for three values of K/κ at each of three latitudes. It indicates that the ratio of the eddy diffusivities influences the magnitude of the oscillation more than the time at which the maximum occurs. As noted above, the amplitude profile at 30° is probably not realistic and the upper boundary condition should be modified at this latitude. As the ratio increases, the amplitude of the wind response decreases at each latitude.

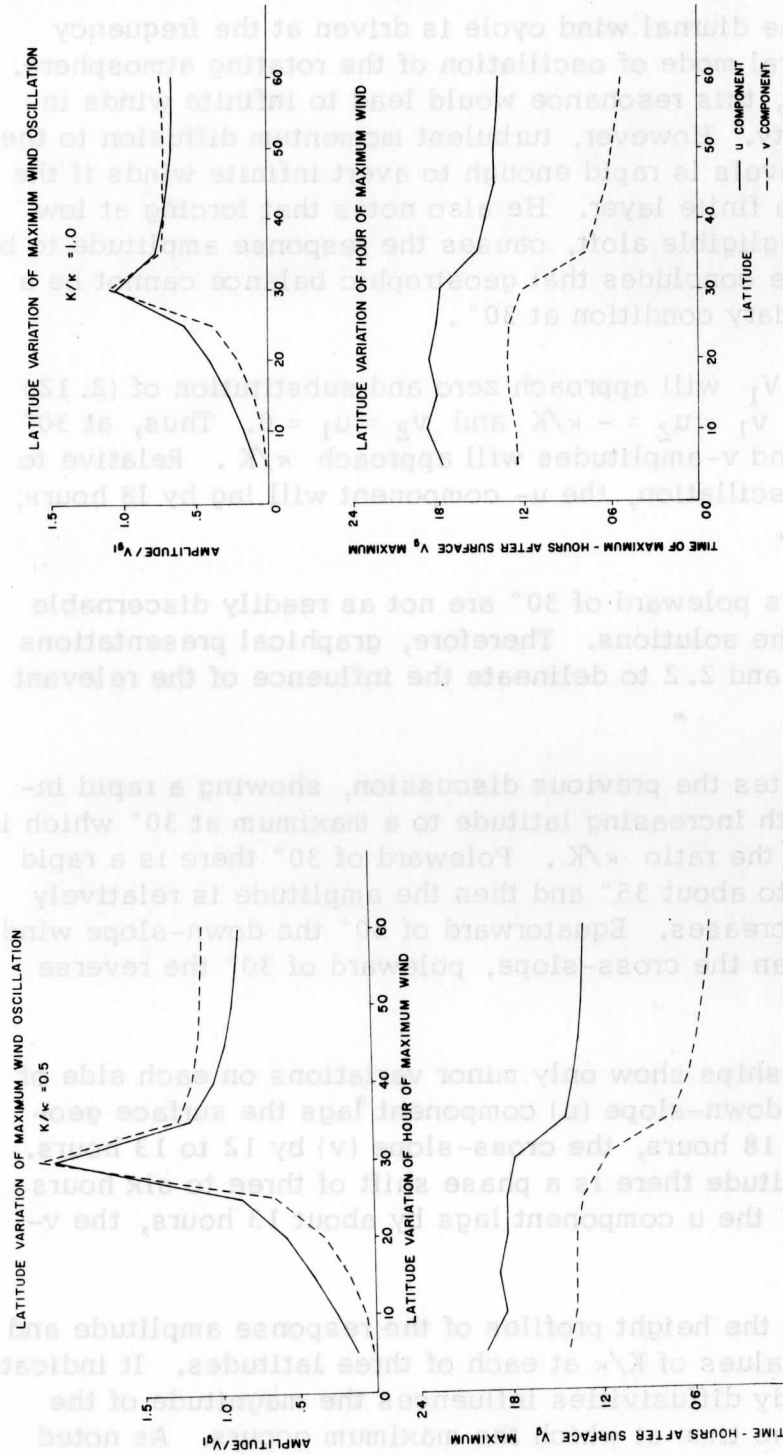

Fig. 2.1. Latitudinal variation of theoretical thermo-tidal response at level of maximum wind for values of ratio of eddy diffusivities of momentum and heat, K/κ, of 0.5 and 1.0.

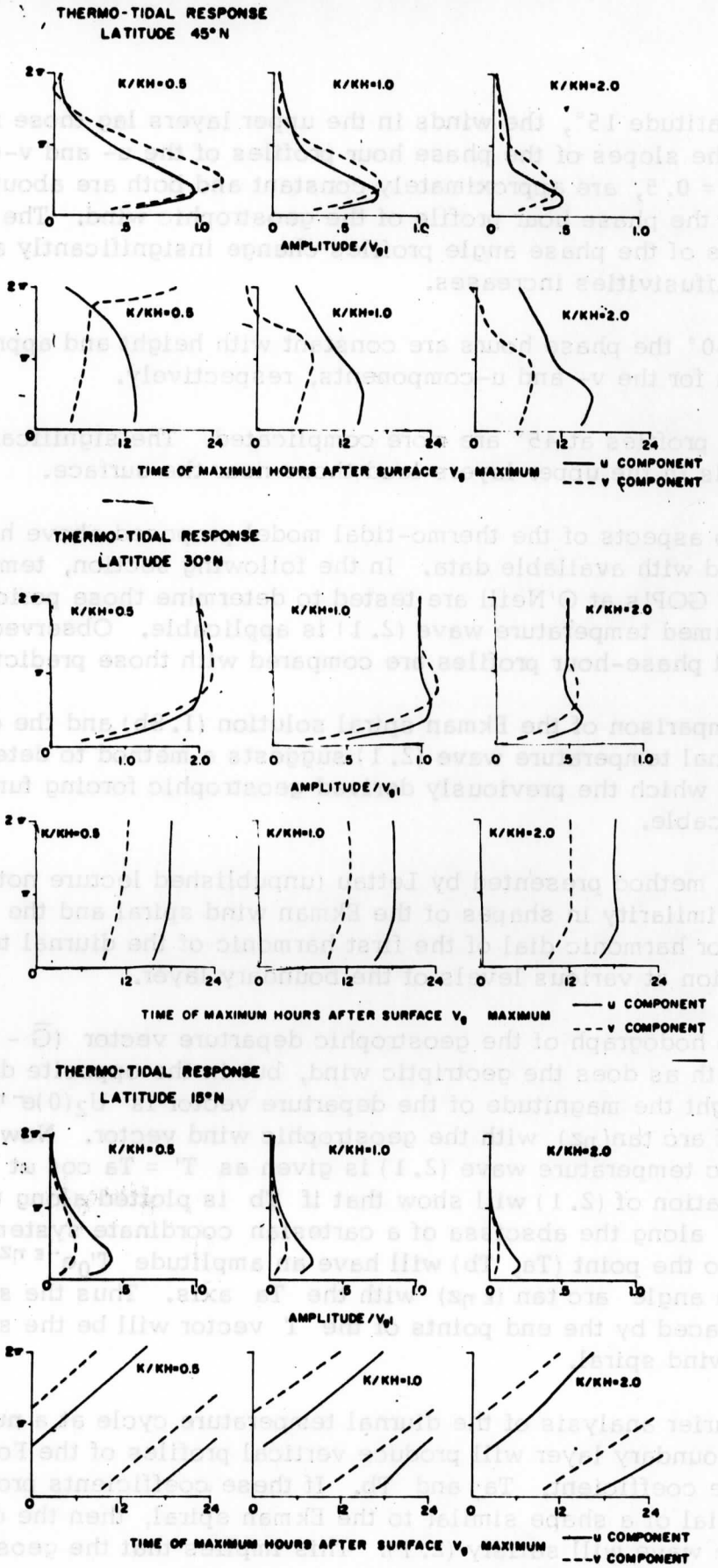

Fig. 2.2. Vertical variation of thermo-tidal wind responses at latitudes 45 N, 30 N and 15 N and for values of K/κ of 0.5, 1.0 and 2.0.

At latitude 15°, the winds in the upper layers lag those near the surface. The slopes of the phase hour profiles of the u- and v-components, for $K/\kappa = 0.5$, are approximately constant and both are about equal to the slope of the phase hour profile of the geostrophic wind. The vertical gradients of the phase angle profiles change insignificantly as the ratio of the diffusivities increases.

At 30° the phase hours are constant with height and approach 12 and 18 hours for the v- and u-components, respectively.

The profiles at 45° are more complicated. The significant fact is that the winds in the upper layers lead those near the surface.

Two aspects of the thermo-tidal model proposed above have been compared with available data. In the following section, temperature data from six GOP's at O'Neill are tested to determine those periods for which the assumed temperature wave (2.1) is applicable. Observed wind amplitude and phase-hour profiles are compared with those predicted.

Comparison of the Ekman spiral solution (1.8b) and the expression for the diurnal temperature wave (2.1) suggests a method to determine those days for which the previously derived geostrophic forcing function derived is applicable.

The method presented by Lettau (unpublished lecture notes) is based on the similarity in shapes of the Ekman wind spiral and the "temperature spiral" or harmonic dial of the first harmonic of the diurnal temperature oscillation at various levels of the boundary layer.

The hodograph of the geostrophic departure vector $(\bar{G} - \bar{V})$ traces the same path as does the geotriptic wind, but in the opposite direction. At any height the magnitude of the departure vector is $U_2(0)e^{-\eta z}$ making an angle of arc $\tan(\eta z)$ with the geostrophic wind vector. Now if the first harmonic temperature wave (2.1) is given as $T' = Ta \cos \omega t + Tb \sin \omega t$, manipulation of (2.1) will show that if Tb is plotted along the ordinate and Ta along the abscissa of a cartesian coordinate system, then the vector to the point (Ta, Tb) will have an amplitude $T'_0 e^{-\varepsilon \eta z}$ and will make an angle arc $\tan(\varepsilon \eta z)$ with the Ta axis. Thus the shape of the curve traced by the end points of the T vector will be the same as the Ekman wind spiral.

Fourier analysis of the diurnal temperature cycle at a number of levels in the boundary layer will produce vertical profiles of the Fourier cosine and sine coefficient, Ta and Tb. If these coefficients produce a harmonic dial of a shape similar to the Ekman spiral, then the diurnal temperature wave will satisfy (2.1). This implies that the geostrophic forcing function can be described by (2.2).

Figure 2.3a presents curves of the amplitude and phase angles determined from Fourier analysis applied to temperature data of the second, fifth and six GOP at O'Neill (Tables 7.2a, for each GOP). Figure 2.3b presents the same curves for the first, third and seventh GOP.

It is evident from Figure 2.3 that the shape of the harmonic dials for the periods depicted in Fig. 2.3a correspond more closely to the Ekman spiral than those in Fig. 2.3b.

The observation periods at O'Neill will be divided as follows: a first category includes periods 2, 5 and 6 during which the geostrophic forcing function can be approximated by that previously derived, and a second category, periods 1, 3 and 7, during which it cannot.

Figure 2.4 presents the first harmonic amplitude and phase profiles for the u- and v-components in the geographic coordinate system as determined from Fourier analysis of the representative winds at each level. This figure shows that the first category yields a rather pronounced maximum in each component amplitude profile, with a positive vertical shear below the level of maximum amplitude of the order of 10^{-2} sec^{-1}.

The wind data of the second category produce less pronounced amplitude maxima, smaller values of shear below the levels of maxima, or both. An exception is the u-amplitude profile of GOP 7 which has a rather pronounced maximum and vertical shear of the order of 10^{-2} sec^{-1}.

The phase characteristics of the two categories also differ. In each of the observation periods of the second category, the v-phase profile changes vertically with the upper level winds lagging those in the lower level. The u-component has a nearly constant phase near the ground. Above a few hundred meters it decreases with height so that the upper winds lead the lower winds. The combination of these two characteristics produces a "cross-over" of the two phase profiles so that at some height below 2 km the u-component of the wind has a maximum earlier than the v-component.

The phase profiles of the first category show no such cross-over. Although there is some change of slope of the v-component phase in the second GOP, the phase profiles of this category are generally characterized by decreasing phase change with height and by the v-amplitude maximum occurring roughly six hours earlier than the u-maximum.

Comparison of Fig. 2.2 and 2.3b shows that the amplitude of the response function decreases more rapidly than the observed winds in the upper levels of the boundary layer.

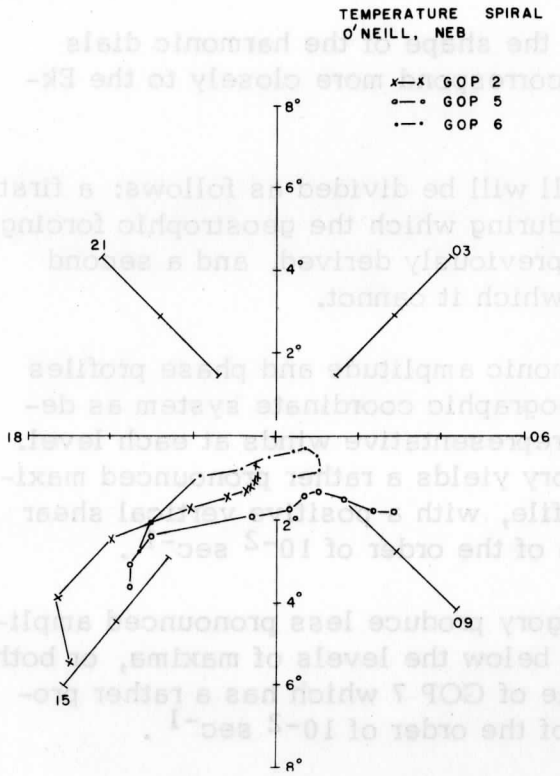

Fig. 2.3a. Properties of the first harmonic of the temperature oscillation at O'Neill, Neb. on a harmonic dial for General Observation Periods of the first category. Distance from origin is in °C, angle from vertical in hours true local time.

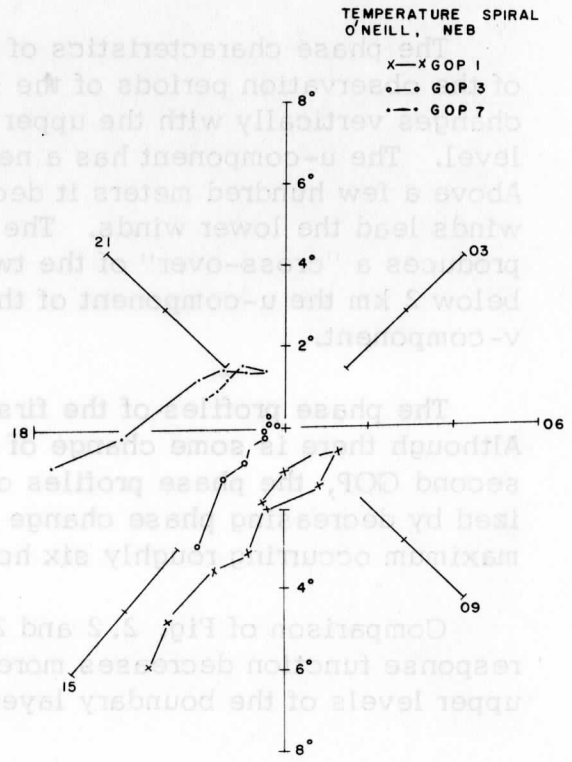

Fig. 2.3b. (right)
Same as Fig. 2.3a except for periods of second category.

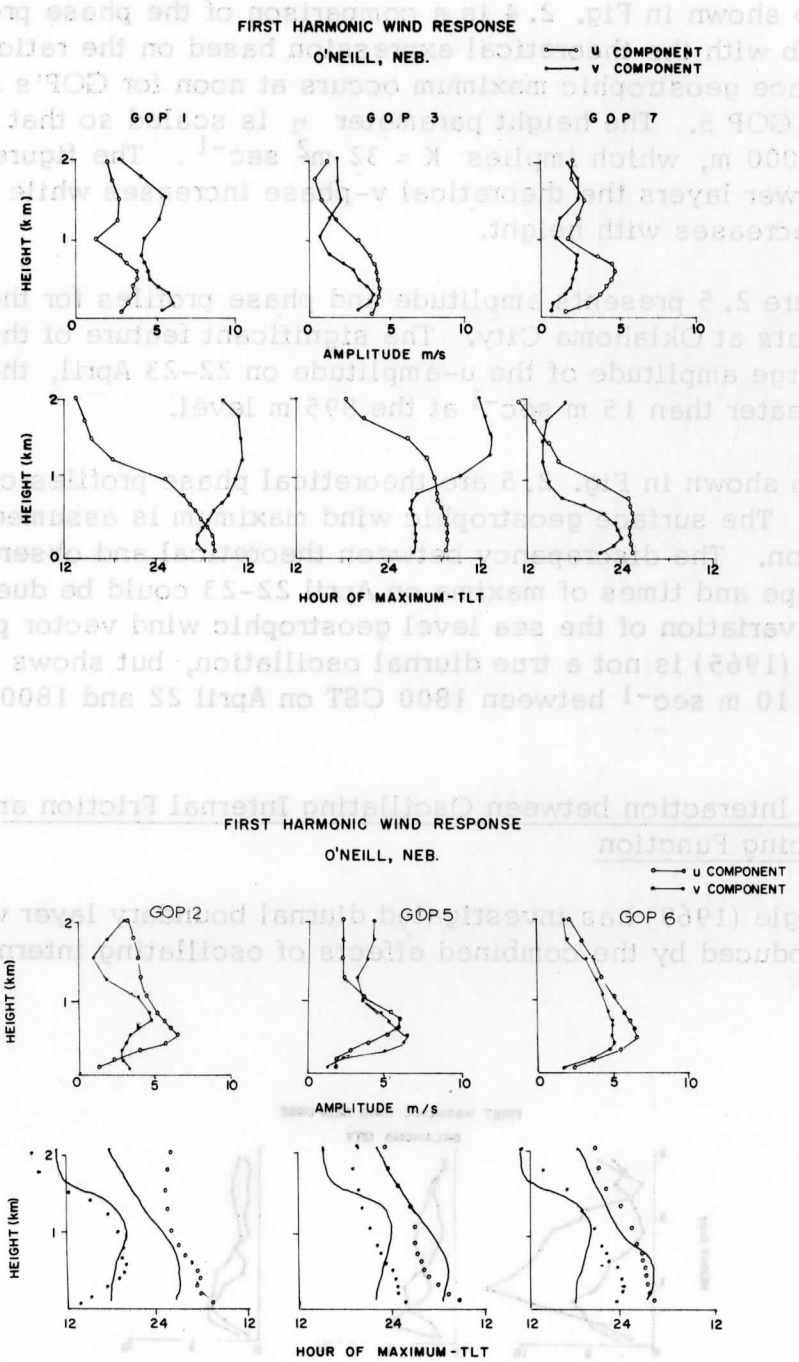

Fig. 2.4. First harmonic amplitude and phase characteristics of wind oscillation at O'Neill, Neb. Upper figure is for periods of second category, lower figure for periods of first category. Theoretical profiles are shown in lower figure as solid lines.

Also shown in Fig. 2.4 is a comparison of the phase profile of Fig. 2.3b with the theoretical expression based on the ratio $K/\kappa = 1$. The surface geostrophic maximum occurs at noon for GOP's 2 and 6, at 1700 for GOP 5. The height parameter η is scaled so that $\eta z = 2\pi$ at $z = 2000$ m, which implies $K = 32\ m^2\ sec^{-1}$. The figure shows that in the lower layers the theoretical v-phase increases while the observed phase decreases with height.

Figure 2.5 presents amplitude and phase profiles for the three observed jets at Oklahoma City. The significant feature of these profiles is the large amplitude of the u-amplitude on 22-23 April, the maximum being greater than 15 m sec^{-1} at the 895 m level.

Also shown in Fig. 2.5 are theoretical phase profiles calculated for $K/\kappa = 1$. The surface geostrophic wind maximum is assumed to occur at local noon. The discrepancy between theoretical and observed profiles in both shape and times of maxima on April 22-23 could be due to the fact that the variation of the sea level geostrophic wind vector presented by Hoecker (1965) is not a true diurnal oscillation, but shows a difference of about 10 m sec^{-1} between 1800 CST on April 22 and 1800 on April 23.

3. The Interaction between Oscillating Internal Friction and Geostrophic Forcing Function

Paegle (1969) has investigated diurnal boundary layer wind oscillations produced by the combined effects of oscillating internal friction

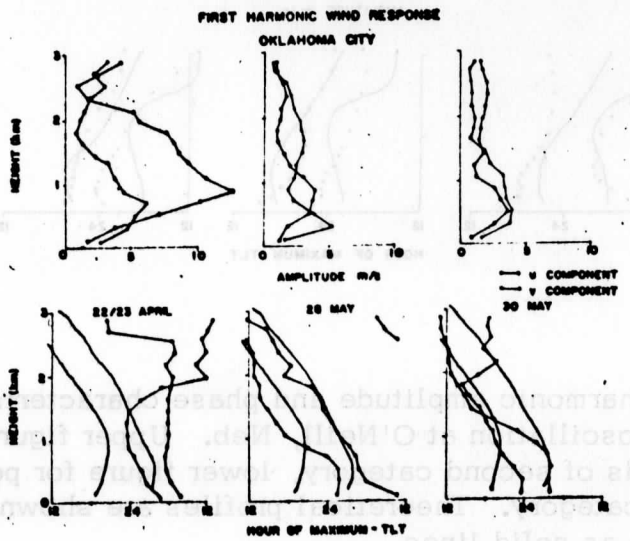

Fig. 2.5. Same as Fig. 2.4 except for Oklahoma City.

and geostrophic wind. He considered two cases in which K was constant with height but varied with time. He notes that the gross features of the hodographs resulting from a step function and from a sinusoidal time variation in K are similar. Therefore, he concludes that the simple sinusoidal time variation in K may be adequate for boundary layer wind studies. Paegle's major conclusion is that a "large day to night eddy viscosity fluctuation gives a nocturnal speed maximum in a strong southerly flow, even with counteracting thermal wind effect at low levels. The resulting speed oscillation is smaller than that which arises from the eddy viscosity alone. However, he calculated a wind response with a maximum two to three hours after the daytime geostrophic wind maximum; therefore, in his model, the effects of oscillating K and G would be opposing each other.

If, however, the wind oscillation produced by a time varying G alone were in phase with the oscillation produced by a time varying K alone, we would expect the wind response due to the combined effects to be enhanced.

The following derivation rather boldly truncates the wind response to the 24-hour mean and the first two harmonics. While this approach lacks Paegle's mathematical sophistication, it should produce the broad outlines of the combined effects of oscillations in K and G.

Paegle (1969) has shown the simple sinusoidal time variation in K is probably adequate for models such as the one to be developed. Therefore, assume

$$K = \bar{K}(1 + 2k \cos \omega t) \tag{3.1a}$$

where k, $0 \leq k \leq 0.5$, is the half amplitude of the oscillation in K and for simplicity the time of maximum is assumed to coincide with the time of maximum surface temperature. The geostrophic forcing function remains given by (2.4) and (2.5). Equation (3.1a) written in complex notation is

$$K = \bar{K}[1 + ke^{i\omega t} + ke^{-i\omega t}]. \tag{3.1b}$$

The 24-hour mean and the first and second harmonics of the wind will be the assumed response, and thus

$$V = \bar{V} + V_1 e^{i\omega t} + V_2 e^{-i\omega t} + V_3 e^{2i\omega t} + V_4 e^{-2i\omega t}. \tag{3.2}$$

Substitution of (3.1b) and (3.2) into (1.5) and separating terms into identical powers of $e^{in\omega t}$ $(-2 \leq n \leq 2)$ results in five ordinary differential equations for the terms in $\bar{V}$,

$$\bar{V}_{zz} - 2i\eta^2 \bar{V} + kV_{1zz} + kV_{2zz} = 2i\eta^2 \bar{G}$$

$$k\bar{V}_{zz} + V_{1zz} - 2i\eta^2\alpha^2 V_1 + kV_{3zz} = 2i\eta^2 G_1$$

$$k\bar{V}_{zz} + kV_{1zz} + kV_{2zz} - 2i\eta^2\beta^2 V_2 + kV_{4zz} = -2i\eta^2 G_2$$

$$+ V_{3zz} - 2i\eta^2\gamma^2 V_3 = 0$$

$$kV_{2zz} + V_{4zz} - 2i\eta^2\delta^2 V_4 = 0 \qquad (3.3a)$$

where in this case $\eta^2 = f/2\bar{K}$ and $\gamma^2 = 1 \delta 2\omega/f$, $\delta^2 = 1 - 2\omega/f$. The produce of the oscillating portion of K with the terms of V_{zz} is the oscillating internal friction and introduces coupling between the five equations of (3.3). This acts so that there is mutual coupling between a given harmonic and the harmonics one higher and one lower in number. Because of the algebraic complexity of the characteristic equation of the set of equations (3.3), a Fortran program was written for the University of Wisconsin Computing Center CDC-3600 computer. This program computed solutions using the "Basic Unified Matrix Package" (BUMP). In matrix notation, the set (3.3) can be written

$$[A]\,[V]_{zz} - 2i\eta^2\,[B][V] = -2i\eta^2\,[G] \qquad (3.3b)$$

where the following matrices are defined:

$$[A] = \begin{bmatrix} 1 & k & k & 0 & 0 \\ k & 1 & 0 & k & 0 \\ k & 0 & 1 & 0 & k \\ 0 & k & 0 & 1 & 0 \\ 0 & 0 & k & 0 & 1 \end{bmatrix}, \quad [V] = \begin{bmatrix} \bar{V} \\ V_1 \\ V_2 \\ V_3 \\ V_4 \end{bmatrix},$$

$$[G] = \begin{bmatrix} \bar{G} \\ G_1 \\ G_2 \\ 0 \\ 0 \end{bmatrix} \quad \text{and} \quad [B] = \begin{bmatrix} 1 & & & & \\ & \alpha^2 & & & \\ & & \beta^2 & & \\ & & & \gamma^2 & \\ & & & & \delta^2 \end{bmatrix} \qquad (3.3c)$$

Multiplying by $[A]^{-1}$, the inverse matrix of [A],

$$[V]_{zz} - 2i\eta^2\,[A]^{-1}\,[B]\,[V] = -2i\eta^2\,[A]^{-1}\,[G]\ . \qquad (3.4)$$

This is the basic form of the set of differential equations (3.3) (Kaplan, 1958), and it was this form which was solved with the Fortran program.

The Fortran program numerically solved for the complex wind response for the 24-hour mean wind and the amplitude and phase profiles for the first and second harmonic of the wind response. The response of the 24-hour mean and first harmonic wind is given by (2.8) and (2.10). Similarly, the amplitudes and phase hours of the second harmonic will be given by

$$\begin{aligned} u\ amp_2 &= (u_3^2 + u_4^2)^{1/2} \\ v\ amp_2 &= (v_3^2 + v_4^2)^{1/2} \end{aligned} \tag{3.5}$$

and

$$u\text{-phase}_2 = \pi/6 \arctan(u_4/u_3)$$

$$v\text{-phase}_2 = \pi/6 \arctan(v_4/v_3),$$

where

$$u_3 = RE(V_3 + V_4) \qquad v_3 = IM(V_3 + V_4)$$

$$u_4 = IM(V_4 - V_3) \qquad v_4 = IM(V_3 - V_4).$$

Figure 3.1 presents the response of the mean wind to the combined effects of oscillating eddy momentum diffusivity and oscillating geostrophic forcing function. The 24-hour mean geostrophic wind is assumed constant with height in the boundary layer with a value of 10 m sec^{-1}. The oscillating portion of the geostrophic forcing function has an amplitude of 5 m sec^{-1} and oscillates parallel to the mean geostrophic wind.

The figure shows that the modification of the Ekman spiral is relatively small as k increases from zero to 0.25. However, as k increases from 0.25 to its limiting value of 0.5, the hodograph becomes quite distorted. At latitude 45 N the spiral becomes more rounded and approaches the geostrophic level with a curvature which is the reverse of the Ekman spiral in the upper levels. At latitude 35 N the mean spiral is even more distorted. The winds just above the earth's surface actually flow opposite to the mean geostrophic wind direction—a rather unlikely situation.

Figures 3.2 and 3.3 depict the amplitudes and phase profiles of the two harmonics of wind response defined by the differential equation (5.4). Figure 3.2 shows the response for latitude 35°; Fig. 3.3 that for 45°. In each case the diffusivities for momentum and heat are assumed equal.

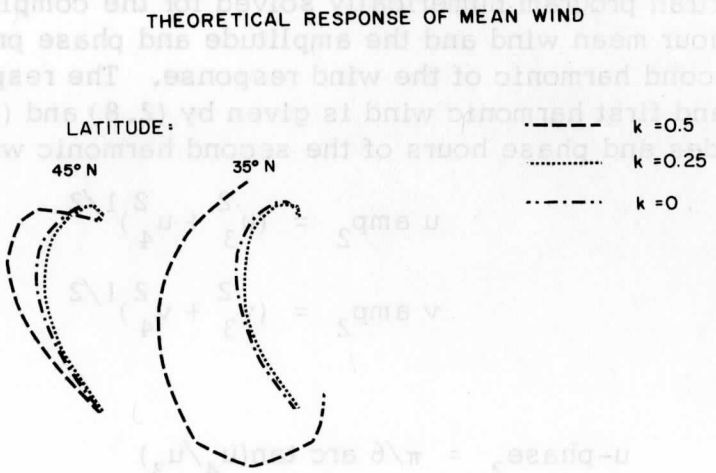

Fig. 3.1. Theoretical response of mean wind to oscillating geostrophic forcing and eddy diffusivity. Mean geostrophic wind is assumed constant with height.

The response function at latitude 35 N shows that the effect of the oscillating diffusivity is to increase the amplitude of the first harmonic at all levels, the amplitude of the wind response increasing with the amplitude of the oscillation of diffusivity. The u-amplitude increases to a limiting value of 1.8 times the amplitude of the surface geostrophic wind oscillation when the range of K varies from zero to twice the average value. The limiting value of the v-amplitude is about 1.75 times G_0.

Both the u- and v-phase profiles of the first harmonic change insignificantly in the upper layers as k increases from zero to 0.25. In the lower part of the boundary layer the phase increases by about two hours for the same increase in k. However, as k increases from 0.25 to its limiting value of 0.5, both the u- and v-profiles show phase shift of 12 to 15 hours.

At latitude 45 N the first harmonic wind response to the combined effects of oscillating internal friction and geostrophic forcing function are confusing. Figure 2.2 shows that as k increases from zero to 0.1, the amplitude of the wind response decreases, the u-amplitude decreasing from 0.65 Ug to 0.25 Ug and the v-amplitude decreasing from about 0.65 Ug to 0.1 Ug. The amplitude profiles for k =0.25 and 0.5 show a similar qualitative relationship to the profiles for k = 0 as those at latitude 35 N, i.e., the wind response amplitudes increase with increasing k.

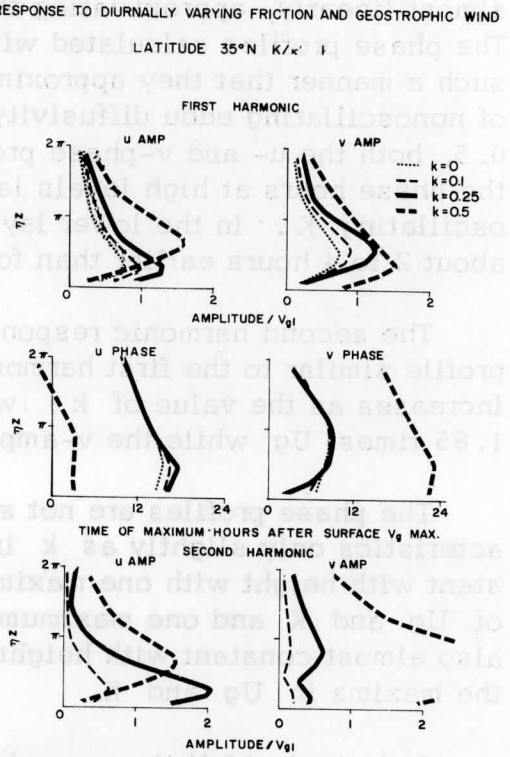

Fig. 3.2. Theoretical characteristics of first and second harmonic of wind response to combined effects of geostrophic wind and eddy momentum oscillations, latitude 35 N.

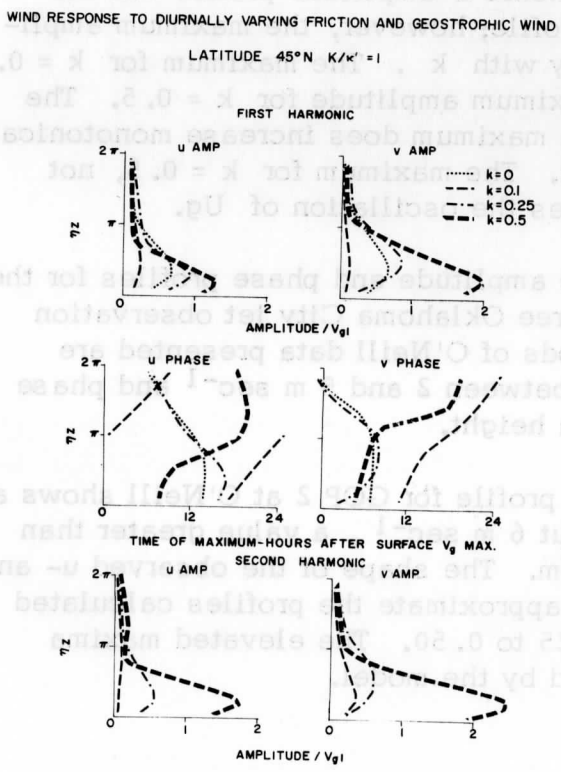

Fig. 3.3. Same as Fig. 3.2 except for latitude 45 N.

The phase profiles show an even more confusing variation with changing values of k . As k goes from zero to 0.1 the shapes of the u- and v-phase profiles are modified so that the phase hour increases almost linearly, approximating the phase profile of the geostrophic wind. The phase profiles calculated with k = 0.5 shift in time and change in such a manner that they approximate the profiles calculated on the basis of nonoscillating eddu diffusivity. As k grows to its limiting value of 0.5, both the u- and v-phase profiles change slope so vehemently that the phase hours at high levels lags 12 to 18 hours behind those for non-oscillating K . In the lower layers, the phase angle for k = 0.5 is only about 2 to 4 hours earlier than for k = 0.

The second harmonic response amplitude at latitude 45 N has a profile similar to the first harmonic amplitude. The maximum amplitude increases as the value of k ; with k = 0.5 the u-amplitude is about 1.85 times Ug while the v-amplitude is almost 2.5 times Ug .

The phase profiles are not shown here; however, they change characteristics only slightly as k increases. The u-profile is nearly constant with height with one maximum in phase synchronous with the maxima of Ug and K and one maximum about 12 hours later. The v-phase is also almost constant with height with maxima about 8 and 20 hours after the maxima in Ug and K.

At latitude 35 N the second harmonic u-amplitude profile has the same shape as the first amplitude profile; however, the maximum amplitude does not increase monotonically with k . The maximum for k = 0.25 being about 25% greater than the maximum amplitude for k = 0.5. The second harmonic v-amplitude profile maximum does increase monotonically with k , but has a double maximum. The maximum for k = 0.5, not shown on the graph, is almost 5 times the oscillation of Ug.

Figures 3.4 and 3.5 present the amplitude and phase profiles for the O'Neill GOP's 2, 5 and 6 for the three Oklahoma City jet observation days, respectively. The three periods of O'Neill data presented are characterized by amplitude maxima between 2 and 5 m sec^{-1} and phase profiles approximately constant with height.

The second harmonic amplitude profile for GOP 2 at O'Neill shows a maximum in the v-component of about 6 m sec^{-1} , a value greater than the first harmonic amplitude maximum. The shape of the observed u- and v-amplitude profiles for this period approximate the profiles calculated for 45° latitude and a k value of 0.25 to 0.50. The elevated maxima observed for GOP 5 are not predicted by the model.

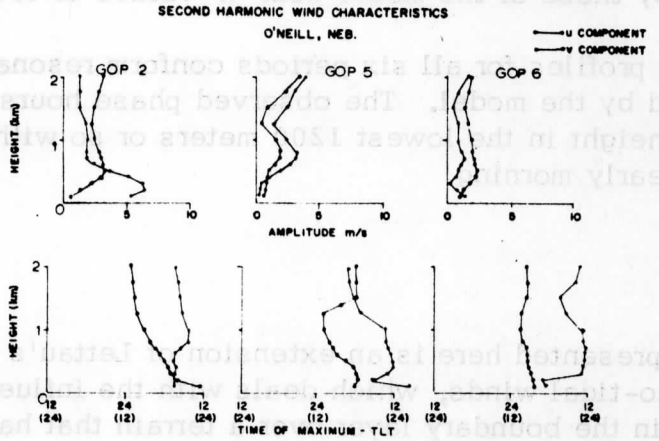

Fig. 3.4. Profiles of second harmonic amplitude and phase profiles at O'Neill, Neb.

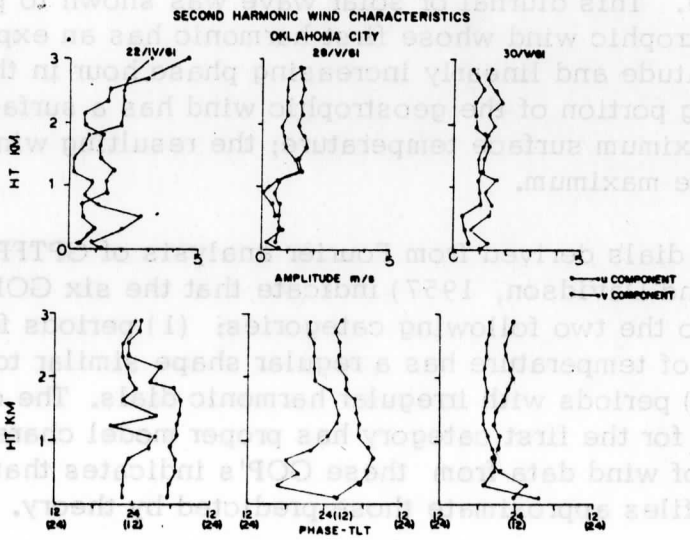

Fig. 3.5. Same as Fig. 3.4 except for Oklahoma City.

The amplitudes for GOP 6 and for the three days of Oklahoma City data (Fig. 3.5) in general vary from about 1 to 3 m sec^{-1} and show no pronounced maxima in the lowest kilometer. These amplitude profiles are approximated by those of the model with k values of 0.1 to 0.25.

The phase profiles for all six periods conform resonably well with those predicted by the model. The observed phase hours are essentially constant with height in the lowest 1200 meters or so with maxima in the afternoon and early morning.

4. Summary

The work presented here is an extension of Lettau's (1964, 1967) model of thermo-tidal winds, which deals with the influence of the diurnal heating cycle in the boundary layer over a terrain that has a large-scale topographical gradient. The development has included diurnal oscillations of the wind components as influenced by the solar heating cycle, and the interaction of oscillation in internal friction and geostrophic wind.

A model of the diurnal thermo-tidal wind is developed with an assumed diurnal temperature wave characterized by an amplitude with exponential height decrease and phase hour with linear increase normal to a sloping terrain surface. This diurnal or solar wave was shown to produce an oscillating geostrophic wind whose first harmonic has an exponentially decreasing amplitude and linearly increasing phase hour in the vertical. The oscillating portion of the geostrophic wind has a surface maximum at the time of maximum surface temperature; the resulting wind oscillation has a nighttime maximum.

Harmonic dials derived from Fourier analysis of GPTFP temperature data (Lettau and Davidson, 1957) indicate that the six GOP's studied can be divided into the two following categories: (1) periods for which the harmonic dial of temperature has a regular shape similar to the Ekman spiral, and (2) periods with irregular harmonic dials. The diurnal temperature wave for the first category has proper model characteristics, and analysis of wind data from these GOP's indicates that the amplitude and phase profiles approximate those predicted by theory.

Harmonic dials of temperature spirals for the periods in the second category do not have shapes approximating the Ekman spiral; thus these temperature waves do not have the form assumed in the model. The characteristics of the wind oscillations during these periods do not conform with prediction by the thermo-tidal wind model.

Finally, a tentative extension to include effects of diurnal oscillations of internal friction is developed. The interaction of a diurnally varying eddy diffusivity for momentum and the diurnally oscillating geostrophic wind enhances the amplitude of the first harmonic wind response and generates a second harmonic in the wind oscillation. The coupling of the equations expressing the mean wind and the two harmonics of the wind oscillation results in highly complicated diurnal variations which are only partially clarified by the present method of solution.

5. Concluding Remarks

One contribution was to demonstrate in detail how a diurnal geostrophic wind oscillation which culminates in the afternoon can produce a wind response with a maximum at night. This result has resolved certain discrepancies between previous solutions presented by Lettau (1964, 1967) and by MacKay (1969) based on geostrophic forcing functions with nighttime surface maxima and diurnal oscillations of actual surface geostrophic wind derived from analysis of previous field observations by Hoecker (1965) and Sangster (1967) which indicate surface maxima in the afternoon.

The results of Sections 2 and 3 contradict Paegle's (1969) conclusions that the effect of the geostrophic wind oscillation cannot explain the nocturnal southerly jets observed over the Great Plains and also that, when oscillations in K and G are specified together the effect of variable K predominates, with the wind response amplitude less than the response to a variable K alone. The main difference between Paegle's attempt to model the influence of the geostrophic wind oscillation and the attempt presented here is that Paegle ignored possible vertical phase changes in the geostrophic forcing function.

Holton (1967) proposed a thermal forcing function similar to the mechanism suggested here. His predicted wind response phases appear too early compared with available observations. It seems, however, that if Holton's phase hours were specified with reference to the surface geostrophic wind maximum instead of the surface temperature maximum, agreement between predicted and observed wind response would be improved.

Further study into the driving mechanism of the thermo-tidal wind should include theoretical investigation of the apparent lag between the maximum temperature and geostrophic wind at the surface of the sloping terrain.

The main contribution of Paegle's investigation is his modeling of the contribution of the nonlinear acceleration terms to boundary layer wind

oscillations. Understanding of these oscillations and associated mesoscale weather phenomena would be enhanced by incorporating a geostrophic forcing similar to that suggested here into Paegle's model which includes the inertial accelerations neglected in this thesis.

Analysis of the combined effects of diurnally oscillating internal friction and geostrophic wind is tentative and insufficient to define adequately the latitudinal variation of the first and second harmonic wind response. A further refinement to the model presented here is the use of more sophisticated Gaussian quadrature techniques as done in similar work by Ooyama (1957) and by Paegle. Further refinement could also be made in the mathematical form of K. Buajitti and Blackadar (1957) showed that the agreement between theoretical prediction and observed wind is improved when both the mean value of K and its amplitude of diurnal oscillation decrease with height above the surface layer.

The mathematical predictions of the thermo-tidal model conform approximately with available observations over the large-scale terrain slope of the central U. S. However, measurements are desirable to determine whether or not the thermal mechanism proposal here is the sole or driving force of the thermo-todal wind. Miller (personal communication, 1969) suggests that summer LLJ oscillations in the inversion layer over San Francisco Bay might be caused by "see-sawing" of the inversion base due to divergence-convergence cycles in the surface maritime air layer.

An extended observation program similar to the chain of observing stations organized and reported by Hoecker (1963, 1965) but also including hourly or two-hourly temperature soundings at several stations would provide desirable information on time and height variations of the horizontal temperature gradient over sloping terrain. These data combined with the surface variation of geostrophic wind derived by a method similar to Sangster (1967) could document the geostrophic forcing function and would help to confirm or contradict the model presented here.

6. References

Bellamy, J. C., 1965: The use of pressure altitude and altimeter corrections in meteorology. J. Meteor., 2: 1-79.

Bonner, W., 1965: Statistical and kinematical properties of the low-level jet stream. Mesometeorology Research Paper 38, University of Chicago, 54 pp.

Bonner, W. D., 1968: Climatology of the low level jet. Mon. Wea. Rev., 96: 833-850.

Blackadar, A. K., 1957: Boundary layer wind maxima and their significance for the growth of nocturnal inversions. Bull. Amer. Meteor. Soc., 83: 283-290.

Bleeker, W. and M. J. André, 1951: On the diurnal variation of precipitation, particularly over central U. S. A., and its relation to large scale orographic circulation systems. Quart. J. Roy. Met. Soc., 77: 260-271.

Buajitti, K. and A. K. Blackadar, 1957: Theoretical studies of diurnal wind variations in the planetary boundary layer. Q. J. Roy. Meteor. Soc., 83: 486-500.

Darkow, G. and O. Thompson, 1968: Diurnal oscillations of the tropospheric wind field above a low-level jet. J. Atm. Sci., 25: 39-46.

Goualt, J., 1938: Vents en altitude a Fort Lamy (Tchad). Annales de Physique du Globe de la France d'Outre-Mer, 5: 70-91.

Haltiner, G. J., 1959: The diurnal variation of the wind. Tellus, 6: 452-458.

Haltiner, G. J. and F. L. Martin, 1957: Dynamical and Physical Meteorology, McGraw-Hill, New York, 470 pp.

Hering, W. and T. Borden, 1962: Diurnal variations in the summer wind field over the Central United States. J. Atmos. Sci., 19: 81-86.

Hoecker, W. H., 1963: Three southerly low-level jet systems delineated by the weather bureau special pibal network of 1961. Mon. Wea. Rev., 91, 573-582.

Hoecker, W. H., 1965: Comparative physical behavior of southerly boundary-layer wind jets. Mon. Wea. Rev., 93: 133-144.

Holton, J. R., 1967: The diurnal boundary layer wind oscillation above sloping terrain. Tellus, XIX: 199-205.

Jeffreys, H., 1929: On the dynamics of wind. Quart. J. Roy. Met. Soc., 48: 29-46.

Johnson, Jr., W. B., 1966: The geotriptic wind. Bull. Amer. Meteor. Soc., 47: 982.

Jordan, C. L., 1966: On Coriolis and the deflecting force. Bull. Amer. Meteor. Soc., 47: 401.

Kaplan, W., 1958: Ordinary Differential Equations, Addison-Wesley, Reading, Mass. 534 pp.

Lettau, H. H., 1964: Preliminary note on the effects of terrain slope on low-level jets and thermal winds in the planetary boundary layer. Section 4 of Studies of the Effects of Variations in Boundary Conditions on the Atmospheric Boundary Layer, Dept. of Meteorology, University of Wisconsin. Annual Report, Contract DA-36-039-AMC-00878, USAERDA, Fort Huachuca, Arizona.

Lettau, H. H., 1967: Small- to large-scale features of boundary layer structures over mountain slopes. Proc. Symposium on Mountain Meteorology, Colorado State Univ.: 1-74.

Lettau, H. H. and B. Davidson, 1957: Exploring the Atmosphere's First Mile, Two Vol., Pergamon Press, New York and London.

MacKay, K. P., Jr., 1969: Thermo-tidal winds in a barotropic boundary layer. Section 8 of Studies of the Effects of Boundary Modification in Problems of Small Area Meteorology. Second Annual and Final Report. Dept. of Meteorology, Univ. of Wisconsin for Grant DA-AMC-28-043-66-624 ECOM, Fort Huachuca, Arizona.

Ooyama, K., 1957: A study of diurnal variation of wind caused by periodic variation of eddy viscosity. Final Rept. Contract No. AFF(604)-1368 New York Univ., College Of Engineering, 80-135.

Paegle, J., 1969: Studies of Diurnally Periodic Boundary Layer Winds, Ph. D. thesis, University of California, Los Angeles, 56 pp.

Pitchford, K. L. and J. London, 1962: The low-level jet as related to nocturnal thunderstorms over midwest Unived States. J. Appl. Meteor., 1: 43-47.

Sangster, W. E., 1967: Diurnal surface geostrophic wind variations over the Great Plains. Proc. Fifth Conf. Severe Local Storms, St. Louis, Mo., Oct. 19-20, 1967, Greater St. Louis Chapter, Amer. Meteor. Soc.: 8 pp.

Sutton, O. G., 1953: Micrometeorology. McGraw-Hill, New York, 333 pp.

DISTRIBUTION LIST*

DEPARTMENT OF DEFENSE

Defense Documentation Center (30)
ATTN: DDC-TCA
Cameron Station (Bldg 5)
Alexandria, Virginia 22314

Technical Library
Dir. of Defense Research & Engr.
Room 3E-1039, The Pentagon
Washington, D. C. 20301

Director, Defense Atomic Sup. Agcy.
ATTN: Document Library Branch
Washington, D. C. 20305

Department of Defense
Defense Intelligence Agency
ATTN: DIAAP-10A2
Washington, D. C. 20301

Spec. Asst. for Environmental Svcs.
Joint Chiefs of Staff
ATTN: Lt. Col. Hampton
Washington, D. C. 20301

DEPARTMENT OF THE NAVY

Chief of Naval Operations
ATTN: Code 427
Department of the Navy
Washington, D. C. 20325

Naval Ships Systems Command
ATTN: Code 20526 (Tech. Library)
Main Navy Bldg., Room 1528
Washington, D. C. 20325

Director (2)
U. S. Naval Research Laboratory
ATTN: Code 2027
Washington, D. C. 20390

Commanding Officer & Director
U.S. Navy Electronics Laboratory
ATTN: Library
San Diego, California 92152

Commander
U.S. Naval Ordnance Laboratory
ATTN: Technical Library
White Oak, Silver Spring, Md. 20910

Commander Naval Weather Svc. (Code 80)
Washington Navy Yard (Bldg. 200)
Washington, D. C. 20390

Commanding Officer
U.S. Navy Weather Research Facility
Bldg. R-48, U.S. Naval Air Station
Norfolk, Virginia 23511

Commandant, Marine Corps (Code AO4C)
Headquarters, U.S. Marine Corps
Washington, D. C. 20380

Development Cen., ATTN: C-E Div.
Marine Corps Dev. & Educ. Comd.
Quantico, Virginia 22134

Commandant, U.S. Marine Corps (Code AO2F)
Headquarters, U.S. Marine Corps.
Washington, D. C. 20380

Commander
U.S. Naval Weapons Laboratory
ATTN: KXR
Dahlgren, Virginia 22448

Ch., Bureau of Naval Weapons
ATTN: Code FASS
Department of the Navy
Washington, D.C. 20315

Commander, Naval Air Sys. Comd.
Meteorological Div. (AIR-540)
Washington, D.C. 20360

DEPARTMENT OF THE AIR FORCE

Electronic Systems Division (ESTI)(ESSIE)(2)
L. G. Hanscom Field
Bedford, Mass. 01730

AFCRL (CREW-CREU-CRER-CRH) (4)
L.G. Hanscom Field
Bedford, Mass. 01730

*Note: One copy to each addressee unless otherwise indicated. Number of copies indicated in parentheses.

Commander
Air Force Cambridge Res. Labs.
ATTN: CRZW, 1965 Main Street
Waltham, Mass. 02154

DEPARTMENT OF THE ARMY

Chief of Research & Development
Department of the Army
Washington, D. C. 20315

Commanding General
U.S. Army Materiel Command
ATTN: AMCRD-TV
Washington, D. C. 20315

Commanding General
U.S. Army Missile Command
ATTN: AMSMI-RRA, Bldg. 5429
Redstone Arsenal, Alabama 35809

Redstone Scientific Info. Cen.
ATTN: Ch., Document Section
U.S. Army Missile Command
Redstone Arsenal, Alabama 35809

Commanding Officer
Aberdeen Proving Ground
ATTN: Tech. Library, Bldg. 313
Aberdeen Proving Ground, Md. 21005

Commanding General (2)
U.S. Army Combat Dev. Command
ATTN: CDCMR-E & Combat Support Gp.
Fort Belvoir, Virginia 22060

Chief of Research & Development
ATTN: CRD/M
Department of the Army
Washington, D. C. 20310

Commanding Officer
U.S. Army Combat Dev. Command
Communications-Electronics Agency
Fort Monmouth, N. J. 07703

Commander
U.S. Army Research Office (Durham)
Box CM - Duke Station
Durham, N.C. 27706

Commanding Officer
U.S. Army Sec. Agcy. Comb. Dev. Actv.
Arlington Hall Station
Arlington, Virginia 22212

U.S. Army Security Agency
ATTN: OAC of S, Dev.
Arlington Hall Station
Arlington, Virginia 22212

U.S. Army Security Agcy. Proc. Cen.
ATTN: IAVAPC-R&D
Vint Hill Farms Station
Warrenton, Virginia 22186

Technical Support Directorate
ATTN: Technical Library
Bldg. 3330, Edgewood Arsenal
Maryland 21010

Commanding Officer
U.S. Army Nuclear Defense Lab.
ATTN: Library
Edgewood Arsenal, Md. 21010

Harry Diamond Laboratories
ATTN: Library
Connecticut Ave. & Van Ness St.
Washington, D. C. 20438

Commandant
U.S. Army Air Defense School
ATTN: C&S Dept. Msl. Sci. Div.
Fort Bliss, Texas 79916

Commander, FHSUPCOM
ATTN: Technical Reference Div.
Fort Huachuca, Arizona 85613

Commanding General
U.S. Army Munitions Command
ATTN: AMSMU-RE-R
Dover, N. J. 07801

Commanding General (3)
U.S. Army Test & Eval. Command
ATTN: AMSTE-EL, -FA, -NBC
Aberdeen Proving Ground, Md. 21005

Commanding Officer
U.S. Army Cold Regions R&E Lab
ATTN: Library
Hanover, New Hampshire 03755

Commanding General
U.S. Army Natick Laboratories
ATTN: AMXRE-EG
Natick, Mass. 01760

Commanding Officer (2)
U. S. Army Ballistic Research Labs.
ATTN: AMXBR-B & AMXBR-IA
Aberdeen Proving Ground, Md. 21005

Director
U.S. Army Engr. Waterways Exp. Sta.
ATTN: Research Center Library
Vicksburg, Miss. 39180

Director
U.S. Army Munitions Command
Operations Research Group
Edgewood Arsenal, Md. 21010

DISTRIBUTION LIST (Continued)

Commanding Officer
Frankford Arsenal, Bldg. 201-1
ATTN: SMUFA-N3200
Philadelphia, Pa. 19137

Commanding Officer
U.S. Army Picatinny Arsenal
ATTN: SMUPA-TVI
Dover, N. J. 07801

Commanding Officer
U.S. Army Dugway Proving Ground
ATTN: Mr. P. Carlson, Met. Div.
Dugway, Utah 84022

President
U.S. Army Artillery Board
Fort Sill, Oklahoma 73503

Commanding Officer
U.S. Army Combat Dev. Comd.
Artillery Agency
Fort Sill, Oklahoma 73503

Commandant
U.S. Army Artillery & Missile School
ATTN: Target Acquisition Dept.
Fort Sill, Oklahoma 73504

Commandant
U.S. Army Chemical Cen. & School
Micrometeorological Section
Fort McClellan, Alabama 36201

Commandant
U.S. Army Signal School
ATTN: Meteorological Dept.
Fort Monmouth, N. J. 07703

Asst. Ch. of Staff for Force Dev.
CBR Nuclear Operations Dir.
Department of the Army
Washington, D. C. 20310

Asst. Secretary of the Army (R&D)
Department of the Army
ATTN: Deputy Asst. for Army R&D
Washington, D. C. 20315

Commanding Officer
U.S. Army Limited Warfare Lab.
Aberdeen Proving Ground, Md. 21005

Ch., Special Techniques Div.
Unconventional Warfare Dept.
U.S. Army Special Warfare School
Fort Bragg, N.C. 28307

Commanding Officer
Fort Detrick
ATTN: Tech. Library, SMUFD-AE-T
Frederick, Md. 21701

Commanding Officer
Fort Detrick
ATTN: SMUFD-AS-S
Frederick, Md. 21701

Commanding Officer
U.S. Army CBR Oper. Research Grp.
Army Chemical Center, Md. 21401

Commanding Officer
U.S. Army Chemical R&D Labs.
ATTN: Dir., Development Support
Army Chemical Center, Md. 21401

Commanding General
U.S. Army Materiel Command
ATTN: AMCMA-EE
Washington, D. C. 20315

Commanding General
U.S. Army Materiel Command
ATTN: AMCRD-R (H. Cohen)
Washington, D. C. 20315

Commanding Officer
U.S. Army Transportation Res. Cmd.
Fort Eustis, Virginia 23604

President
U.S. Army Arctic Test Board
Ft. Greely, Delta Junction
Alaska 99737

Headquarters
U.S. Army Supply & Maintenance Cmd.
Dover, N.J. 07801

Commanding General
U.S. Army CDC
Combined Arms Group
Ft. Leavenworth, Kansas 66027

Commanding General
U.S. Army Combat Developments Cmd.
Combat Support Group
Ft. Belvoir, Virginia 22060

Commanding General
U.S. Army Munitions Command
ATTN: AMSMU-RE-P
Dover, N.J. 07801

Commanding General
U.S. Army Test & Eval. Comd.
ATTN: NBC Directorate
Aberdeen Proving Ground, Md. 21005

DISTRIBUTION LIST (Continued)

Commanding General
U.S. Army Natick Labs.
ATTN: Earth Sciences Div.
Natick, Mass. 01762

Commanding General
Deseret Test Center, Bldg. 103
ATTN: STEPD-TT-ME(S) Met. Div.
Ft. Douglas, Utah 84113

Commanding General
Fort Detrick
ATTN: Environmental Analysis Ofc.
Frederick, Md. 21701

CG, U.S. Army Electronics Cmd.
ATTN: AMSEL-MR
225 South 18th St.
Philadelphia, Pa. 19103

Headquarters
U.S. Army Combat Dev. Comd
ATTN: CDCLN-EL
Ft. Belvoir, Virginia 22060

USAECOM Liaison Officer
MIT, Bldg. 26, Room 131
77 Massachusetts Ave.
Cambridge, Mass. 02139

USAECOM Liaison Officer
Aeronautical Systems Div.
ATTN: ASDL-9
Wright-Patterson AFB, Ohio 45433

Ch., Atmos. Sci. Tech. Area (20)
ASL, USAECOM, ATTN: AMSEL-BL-RD
Fort Huachuca, Arizona 85613

Ch., Atmos. Sci. Office
Atmos. Sci. Lab.
U.S. Army Electronics Command
White Sands Msl. Range, N. M. 88002

Commanding General (11)
U.S. Army Electronics Cmd.
Fort Monmouth, N. J. 07703

ATTN: AMSEL-EW
AMSEL-ME-NMP-PS
AMSEL-TD-TI
AMSEL-RD-MT

AMSEL-XL-D
AMSEL-NL-D
AMSEL-VL-D
AMSEL-SC
AMSEL-RD-D
AMSEL-RD-LNF

NASA Scientific & Tech. Info. Fac.
ATTN; Acquisitions Br. (S-AK/DL)
P. O. Box 33
College Park, Md. 20740

DASA Info. & Analysis Center
General Electric - Tempo
816 State St.
Santa Barbara, Calif. 93102

Institute of Science & Technology
University of Michigan
P.O. Box 618 (IRIA Library)
Ann Arbor, Mich. 48107

Vela Seismic Info. Center
University of Michigan
P.O. Box 618
Ann Arbor, Mich. 48107

Battelle - Defender Info. Center
Battelle Memorial Institute
505 King Ave.
Columbus, Ohio 43201

Library of Congress
ATTN: Exchange & Gift Div.
Washington, D. C. 20540

Head, Atmos. Sciences Section
National Science Foundation
1800 G Street, N.W.
Washington, D. C. 20550

Chief, Fallout Studies Branch
Division of Biology & Medicine
Atomic Energy Commission
Washington, D. C. 20545

Natl. Cen. for Atmos. Research
NCAR Library, Acquistions - Reports
Boulder, Colorado 80302

OCE, Bureau of Reclamation
ATTN: D755, Bldg. 67
Denver, Colorado 80225

Director, Meteorology Dept.
University of Arizona
Tucson, Arizona 85717

Meteorology Department
San Jose State College
San Jose, California 95113

DISTRIBUTION LIST (Continued)

Dept. of Civil Engineering
ATTN: Dr. J. E. Cermak
Colorado State University
Fort Collins, Colorado 80521

Forest Service Exp. Sta.
ATTN: Mr. M. Martinelli
Rm. 221 Forestry Bldg., CSU
Fort Collins, Colorado 80521

Director, Meteorology Dept.
Florida State University
Tallahassee, Florida 32301

Meteorology Dept.
University of Hawaii
Honolulu, Hawaii 96822

Rosenwald Library
Meteorology Collection
University of Chicago
1101 E, 58th St.
Chicago, Illinois 60637

Dept. of Agronomy
ATTN: Dr. R. H. Shaw
Iowa State University
Ames, Iowa 50010

Director, Meteorology Dept.
University of Michigan
Ann Arbor, Michigan 48104

Director, Meteorology Dept.
Massachusetts Inst. of Technology
Cambridge, Mass. 02138

Director, Meteorology Dept.
St. Louis University
St. Louis, Missouri 63120

Microclimate Investigations
SWC-ARS-USDA
Bradfield Hall, Cornell Univ.
Ithaca, N.Y. 14850

Director
Meteorology Department
Pennsylvania State University
University Park, Pa. 16802

Dept. of Oceanography & Meteorology
Texas A&M University
College Station, Texas 77840

Dept. of Meteorology
University of Utah
Salt Lake City, Utah 84116

Dr. J. A. Businger
Meteorology Department
University of Washington
Seattle, Wash. 99703

Director
Meteorology Department
University of Wisconsin
Madison, Wis. 53705

Department of Soils
University of Wisconsin
ATTN: Dr. C. B. Tanner
Madison, Wis. 53705

Forestry Library
260 Walter Mulford Hall
University of California
Berkeley, Calif. 94704

Commander
AF Cambridge Research Lab.
ATTN: Ch., Boundary Layer Br.
Bedford, Mass. 01730

Argonne National Lab.
ATTN: Mr. Harry Moses, Met. Bldg.
9700 So. Cass Ave.
Argonne, Illinois 60440

Prof. J. E. Pearson
Gen. Engr. Dept., Atmos. Sci. Lab.
University of Illinois
Urbana, Illinois 61801

Brookhaven National Lab.
ATTN: Meteorology Group
Upton, L.I., N.Y. 11973

Dr. Kenneth R. Knoerr
School of Forestry
Duke University
Durham, North Carolina 27706

Prof. W. E. Reifsnyder
School of Forestry
Marsh Hall, 360 Prospect St.
New Haven, Conn. 06511

Dr. Leo J. Fritschen
College of Forestry
University of Washington
Seattle, Washington 98105

ARS, Snake River Cons. Res. Cen.
ATTN: Dr. J. L. Wright
Rt. 1, Box 186
Kimberly, Idaho 83341

Dr. C. H. M. van Bavel
Institute of Life Sciences
Texas A&M University
College Station, Texas 77843

Dr. Raymond E. Leonard
Northeastern Forest Exp. Sta.
SUNY College of Forestry
Syracuse, New York 13210

Institute for Storm Research
The University of St. Thomas
3812 Montrose
Houston, Texas 77006

Director
Pacific SW Forest & Range Exp. Sta.
Box 245
Berkeley, California 94701

Scientific Research Institute
Oregon State University
ATTN: Atmospheric Science Br.
Corvallis, Oregon 97330

Director
Environmental Biology Program
National Science Foundation
Washington, D. C. 20550

Commanding Officer & Director (5)
Atmospheric Sciences Laboratory
U.S. Army Electronics Command
White Sands Missile Range, N.M. 88002

Ofc. of Asst. Ch. of Staff for DS-SSS
Department of the Army
Rm. 3C466, The Pentagon
Washington, D. C. 20315

Ofc. Asst. Sec. of the Army (R&D)
ATTN: Asst. for Research
Rm 3-E-373, The Pentagon
Washington, D. C. 20310

Fresno State College
Atmospheric Water Resources
ATTN: Mr. M.C. Williams
5302 No. Fresno St.
Fresno, Calif. 93726

Director, Meteorology Department
University of California
Los Angeles, Calif. 90052

Dr. E. P. Van Arsdel
College of Agriculture - Plant Sci. Dept.
Texas A&M University
College Station, Texas 77843

Director
U.S. Water Conservation Lab.
4331 E. Broadway
Phoenix, Arizona 85040

Division of Meteorology
National Air Pollution Cont Adm
3820 Merton Drive
Raleigh, North Carolina 27609

Dept of Water Sci & Engr
Attn: Mr. W. O. Pruitt
University of California
Davis, California 95616

Dept of Agr Engr
Attn: Dr. K. L. Coulson
University of California
Davis, California 95616

Office of the Director
Defense Research & Engineering
Attn: Chief, Environmental Sci Div
Room 3-C-128, The Pentagon
Washington, D. C. 20301